ORO-3822-7
December 1970

STRUCTURE - FOUNDATION INTERACTION OF NUCLEAR POWER PLANTS - PHASE I FINAL REPORT

by

R. J. SCAVUZZO

UNITED STATES ATOMIC ENERGY COMMISSION

CONTRACT NO. AT-(40-1)-3822

THE UNIVERSITY OF TOLEDO

TOLEDO, OHIO

ABSTRACT

The overall objective of the work supported by this contract is to determine the extent to which large reactor structures interact with free-field seismic ground motion so as to alter the base motion from free-field values. The purpose of Phase I of this contract is to assess the significance of soil-structure interaction including rocking effects and consequent response spectra for a range of relatively idealized simulations of the structure, the foundation conditions and the input seismic wave form.

Studies under this phase were conducted at The University of Toledo, Toledo, Ohio and IIT Research Institute, Chicago, Illinois. Analytical methods were developed at The University of Toledo to study this phenomenon. A finite element stress wave propagation program, SLAM, was employed at IITRI to study interaction effects. Results of these studies showed that interaction effects are often very significant and should be considered in the seismic design of nuclear power plants. The significance of interaction effects on dynamic loads caused by earthquakes depends upon the soil stiffness, the structure weight and modal properties, and the frequency characteristics of the input wave.

Four technical reports were issued under this phase of work. These reports are as follows:

(1) Scavuzzo, R. J. and D. Raftopoulos. "Literature Review of Structure-Foundation Interaction." USAEC Contract No. AT-(40-1)-3822, Technical Report No. 1, The Research Foundation, University of Toledo, October, 1968

(2) Scavuzzo, R. J. and J. L. Bailey, D. D. Raftopoulos. "Lateral Structure-Foundation Interaction of Nuclear Power Plants During Earthquake Loading," USAEC Contract No. AT-(40-1)-3822, Report No. 2, Research Foundation, Dept. of Mechanical Engineering of The University of Toledo, August, 1969

(3) Scavuzzo, R. J. and D. D. Raftopoulos, J. L. Bailey. "Lateral Structure-Foundation Interaction of Nuclear Power Plants with Large Base Masses." USAEC Contract No. AT-(40-1)-3822, Department of Mechanical Engineering of The University of Toledo, Report No. 3, September 1969

(4) Chiapetta, R. "Effect of Soil-Structure Interaction on the Response of Reactor Structures to Seismic Ground Motion," IIT Research Institute, ORO-3822-4.

TABLE OF CONTENTS

LIST OF FIGURES

LIST OF FIGURES (cont'd)

LIST OF TABLES

NOMENCLATURE

a	Dilatation (P) wave velocity
A	Area of the structure base
b	Shear (S) wave velocity
c	Half the base width
E	Young's modulus
$F(t)$	Lateral force at the base of a structure
$f(t)$	Surface shear stress when $\|x\| < c$
M_o	Base mass
M_j	Effective mass of the j^{th} mode
m_j	The j^{th} structure mass
$u(x, y, t)$	Lateral displacement in the half-space (x-direction)
$u(t)$	Lateral displacement of the center of the base
$u_p(t)$	Free-field lateral displacement at the center of the base
t	Time
V	Rayleigh wave velocity
$\overline{X}_{ij}$	Mode shape for the i^{th} mass and j^{th} mode
$x(t)$	Absolute lateral motion of dynamic mass
$z(t)$	Relative lateral motion of dynamic mass

NOMENCLATURE (cont'd)

$\alpha(t)$	Foundation rotational motion
ω_j	Natural circular frequency of the j^{th} mode
μ	Shear modulus $= \frac{E}{2(1+\nu)}$
ν	Poisson's Ratio
ρ	Ground density

INTRODUCTION

Dynamic loads caused by earthquakes must be considered in the design of nuclear power plants. One of the methods of analysis used to evaluate seismic loads is based on the spectrum response of the ground motion (1, 2, 3, 4). A basic assumption made in the application of this method of analysis is that the spectrum response of the ground motion is not affected by the presence of the structure. The purpose of the work done under Phase I of this contract is to determine the significance of soil-structure interaction including rocking effects and consequent response spectra for a range of relatively idealized simulations of the structure, the foundation conditions and the input seismic wave form and to determine if this effect must be considered in the seismic design of nuclear power plants. In this phase of work, a two-dimensional elastic half space is used to represent the soil. Furthermore, it is assumed that the ground and structure are fully coupled with no slipping. Interaction effects are evaluated by comparing response spectra from calculated foundation motions with response spectra from the free-field (input) motion.

Separate studies of structure foundation interaction were conducted at The University of Toledo (5, 6, 7) and IIT Research Institute, Chicago, Illinois (8). Analytical methods of analysis were developed at The University of Toledo to study this phenomenon. A finite element stress wave propagation program, SLAM, was employed by IITRI to study interaction effects.

A summary of results of these studies is presented herein. In addition, the effect of structure rotation on seismic loads is also evaluated using results of the SLAM calculations. A comparison of SLAM results with the analytical procedures described in Reference (6) is also presented.

DISCUSSION OF RESULTS

Analytical Studies

In the analytical procedures employed at The University of Toledo, the ground is assumed to be a homogeneous elastic two-dimensional half space. Along the free surface, the normal stress is taken to be zero and the shear stress is assumed to vary arbitrarily with time on the interval $-c < x < c$ and is zero outside of this interval (Figure 1). With these boundary conditions transform techniques are used to obtain the solution for the lateral displacement of the origin caused by shear stresses, f(t), which is presented in equation (1)*.

$$u(0,0,t) = -\frac{b}{\mu}\int_0^t f(\tau)d\tau - \frac{b^2}{2\pi c\mu}\int_0^t\int_0^{t-\tau} f(\xi)\ \mathrm{Im}\ g\left(\frac{b\tau}{c}\right)d\xi d\tau \qquad (1)$$

where Im $g(\frac{b\tau}{c})$ is the imaginary part of $g(\frac{b\tau}{c})$. The function g(T) is defined by equation (2).

$$g(T) = \frac{\sqrt{1 - T^2}}{T\left[(\frac{1}{2} - T^2)^2 + T^2\sqrt{\frac{1}{3} - T^2}\sqrt{1 - T^2}\ \right]} \qquad (2)$$

---

*See the nomenclature for a definition of the symbols.

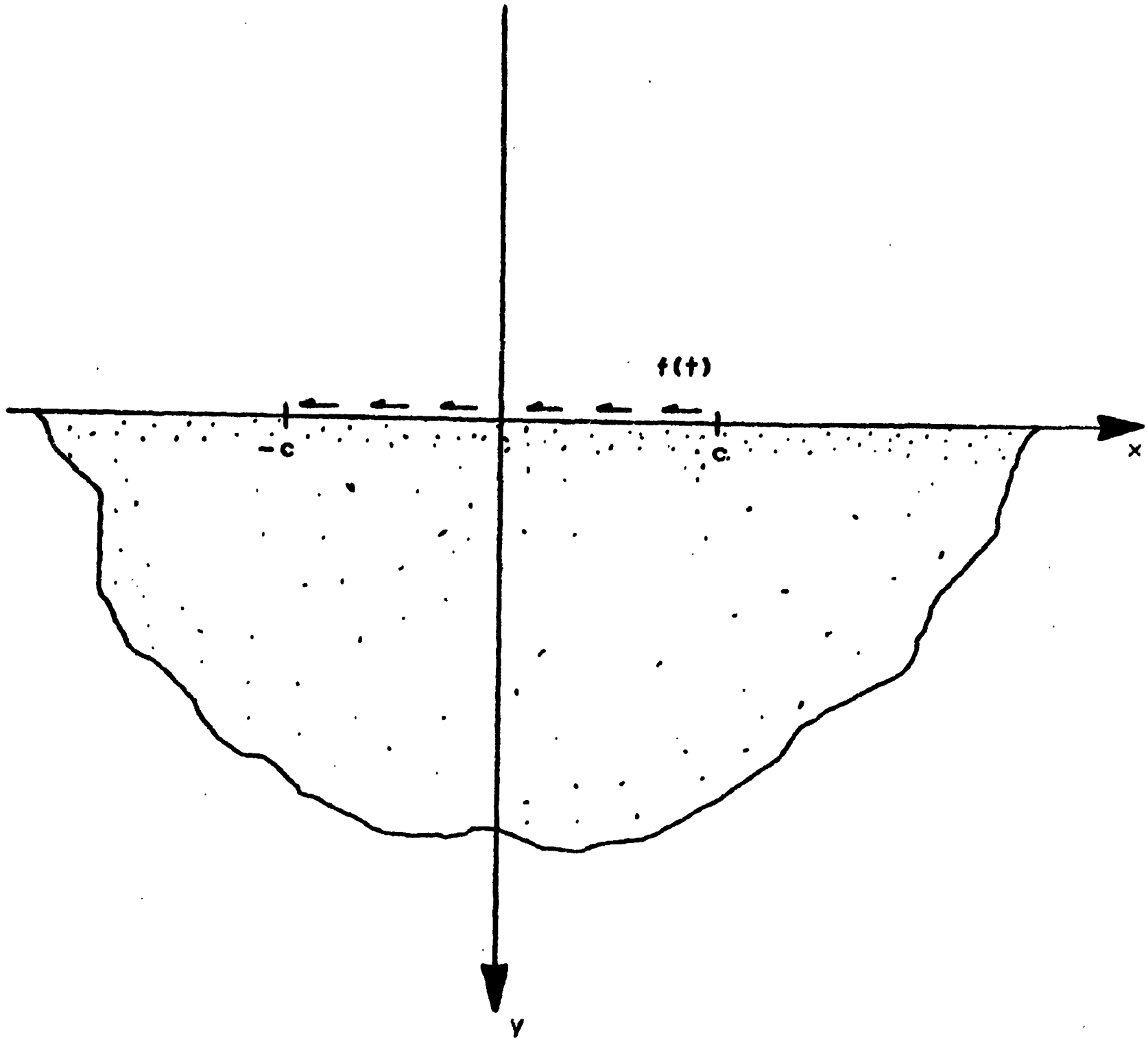

Figure 1 Coordinate system used in the solution to the Lamb problem. A shear stress, f(t), which acts between $\pm$c varies arbitrarily with time. The remaining portion of the surface is stress free. Normal stresses over the entire surface are zero.

The imaginary part of g(T) can be evaluated as (5, 7)

$$\text{Im } g(T) = \begin{cases} 0 & , 0 < T < \frac{1}{\sqrt{3}} \\ \dfrac{3T(1-T^2)\sqrt{T^2-\frac{1}{3}}}{2(T^2-\frac{1}{4})(T^2-\frac{3-\sqrt{3}}{4})(T^2-\frac{3+\sqrt{3}}{4})} & , \frac{1}{\sqrt{3}} < T < 1 \\ -\dfrac{3\sqrt{T^2-1}\left[(T^2-\frac{1}{2})^2 + T^2\sqrt{T^2-\frac{1}{3}}\sqrt{T^2-1}\right]}{2T(T^2-\frac{1}{4})(T^2-\frac{3-\sqrt{3}}{4})(T^2-\frac{3+\sqrt{3}}{4})} & , T > 1 \end{cases} \tag{3}$$

In order to simplify the computations in the inversion of the transformed variables, Poisson's ratio is made equal to 1/4. For this case, $a = \sqrt{3}\ b$ where a is the dilitation wave velocity and b is the shear wave velocity.

The lateral displacement obtained from equation (1) is the displacement caused by the arbitrarily varying shear stress, f(t). In order to obtain the total lateral displacements, the free-field displacement caused by seismic motion, $u_p(t)$, must be added to equation (1). Thus, the equation for the total displacement becomes

$$u(t) = -\frac{b}{\mu}\int_0^t f(\tau)d\tau - \frac{b^2}{2\pi c\mu}\int_0^t\int_0^{t-\tau} f(\xi)\ \text{Im } g\left(\frac{b\tau}{c}\right)d\xi d\tau + u_p(t) \tag{4}$$

Two types of structure were considered in these analytic studies: those without significant base masses and those with base masses. For the case in which the base mass can be neglected, the structural inertia forces can be related to the surface shear stress, f(t), in the following

$$F(t) = -\sum_j M_j \omega_j \int_0^t \ddot{u}(0,0,\tau) \sin \omega_j (t-\tau) d\tau \tag{5}$$

where the effective mass for the j^{th} mode, M_j, is defined by the following equation

$$M_j = \frac{\left(\sum_i \bar{X}_{ij} m_i\right)^2}{\sum_i \bar{X}_{ij}^2 m_i} \tag{6}$$

and $\bar{X}_{ij}$ are the mode shapes (eigenvectors) of the linear elastic N-mass structure fixed at the base and m_i are the concentrated masses.

If a large base mass is considered, equation (5) must be altered as shown in equation (7).

$$F(t) = \sum_j M_j \omega_j \int_0^t \ddot{u}(\tau) \sin \omega_j (t-\tau) d\tau + M_o \ddot{u}(t) \tag{7}$$

where M_o is the base mass.

Interaction equations are developed by substituting either equation (5) or equation (7) into equation (4). In order to obtain an integral equation in terms of acceleration for a structure without a base mass, the second time

derivative of equation (1) is taken. After substitution, the resulting integral equation is

$$\ddot{u}(0,0,t) = -\frac{b}{\mu A}\sum_j M_j\,\omega_j^2\int_0^t \ddot{u}(0,0,\xi)\cos\omega_j(t-\xi)\,d\xi -$$

$$\frac{b^2}{2\pi\mu cA}\int_0^t \sum_j M_j\,\omega_j^2\int_0^{t-\tau}\left[\ddot{u}(0,0,\xi)\cos\omega_j(t-\tau-\xi)\,d\xi\right]\mathrm{Im}\left(g\left(\frac{b\tau}{c}\right)\right)d\tau + \qquad (8)$$

$$\ddot{u}_p(t)$$

Equation (8) is an integral equation of the Volterra type in terms of the foundation acceleration, $\ddot{u}(0, 0, t)$, at the origin of the system. The prescribed function $\ddot{u}_p(t)$ is the lateral free-field acceleration at the origin without a structure present. The modal characteristics of the structure are described by the effective mass, M_j, and circular frequency, ω_j . for each (jth) mode of the system. Foundation geometry is defined by the base area, A, and the effective base half width, c. The elastic properties of the ground are specified by the shear wave velocity, b , and shear modulus, μ .

The integral equation is solved by iteration which is performed numerically at each time interval, t. The digital computer program used in this solution is described and listed in Reference (5).

For a structure with a base mass, the first time derivative of equation (4) is taken and equation (7) is substituted into the result. After rearranging terms the resulting integral equation can be expressed as

$$\ddot{u}(t) = -\frac{1}{M_o}\sum_j M_j\omega_j\int_0^t \ddot{u}(\tau)\sin\omega_j(t-\tau)d\tau - \frac{b}{2\pi c}\int_0^t \ddot{u}(t-\tau)\,\mathrm{Im}\left[g(\frac{b\tau}{c})\right]d\tau$$

$$-\frac{b}{2\pi cM_o}\sum_j M_j\omega_j\int_0^t\int_0^{t-\tau}\ddot{u}(\xi)\;\mathrm{Im}\left[g(\frac{b\tau}{c})\right]\sin\omega_j(t-\tau-\xi)d\xi d\tau \qquad (9)$$

$$+\frac{\mu A}{bM_o}\int_0^t\left[\ddot{u}_p(\tau)-\ddot{u}(\tau)\right]d\tau$$

By comparing equation (9) with equation (8) where the same problem is solved except for the addition of the base mass, it can be noted that the first and third terms contain sines instead of cosines and that two additional terms appear. Numerical interation at each time interval is also used to solve equation (9). A listing of the digital computer program is presented in Reference (6).

Details of the many numerical studies based on equations (8) and (9) are presented in References (5) and (6) respectively. A summary of these results is presented herein.

All numerical studies were based on the same structure which is described in Reference (5). This relatively simple model consists of three masses: a base mass ($2,400,000\ \frac{\text{lb - sec}^2}{\text{ft}}$), a containment vessel mass ($475,000\ \frac{\text{lb - sec}^2}{\text{ft}}$), and an internal structure mass ($310,000\ \frac{\text{lb - sec}^2}{\text{ft}}$) (Figure 2).

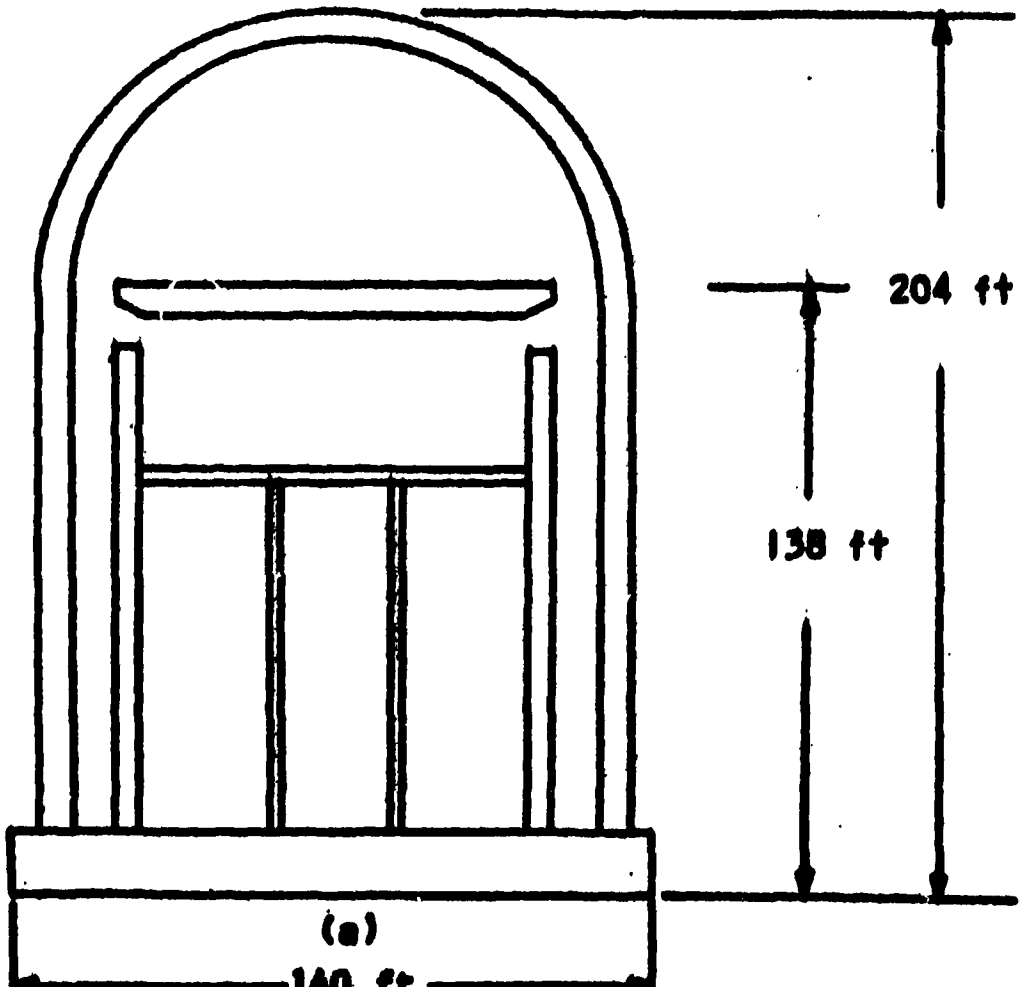

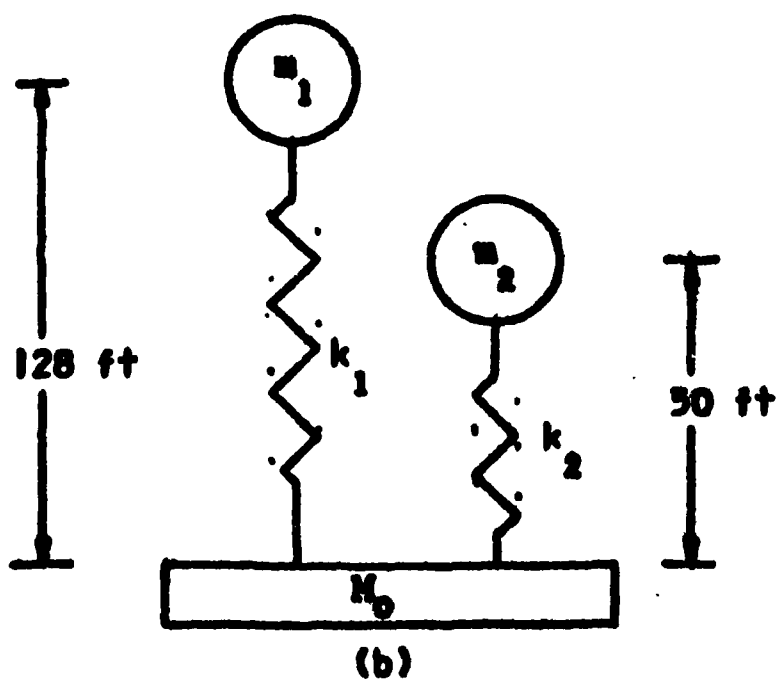

$M_0 = 2400000 \frac{lb\text{-}sec^2}{ft}$

$m_1 = 475000 \frac{lb\text{-}sec^2}{ft}$

$m_2 = 310000 \frac{lb\text{-}sec^2}{ft}$

$k_1 = 0.31 \times 10^9$ lb/ft

$k_2 = 0.30 \times 10^9$ lb/ft

A = 13[illegible] ft^2

Figure 2 The nuclear power plant shown in Figure 2a has been idealized as indicated in Figure 2b. The masses M_o, m_1 and m_2 represent the base, containment vessel, and internal structure, respectively.

The fixed-base frequencies of the containment vessel mass and internal structure mass are approximately 4.0 cps and 5.0 cps respectively. These fixed-base frequencies were varied in some parametric studies in order to determine the significance of structure frequency on interaction effects. In many cases, only the effects of the containment vessel mass were considered.

An ideal free-field acceleration described by equation (10) was used as input to both equation (8) and equation (9) in parametric studies.

$$\ddot{u}_p(t) = \begin{cases} \frac{5t}{8} \sin 10 \pi t & 0 \leq t \leq 0.8 \\ 5\left(\frac{2-t}{14}\right) \sin 10 \pi t & 0.8 < t \leq 2.0 \\ 0 & t > 2.0 \end{cases} \qquad (10)$$

The natural frequency of this ramp sinusoidal function is 5.0 cps and the maximum value of the ramp function is 0.5 g's. This function, $u_p(t)$, is graphed in Figures 3 and 4. In all parametric studies three different values of the ground shear wave velocities were used as input: 500 ft/sec., 1000 ft/sec and 2000 ft/sec. The ground density was always taken to be 100 lbs/ft^3.

Both the input and output accelerations for the containment-vessel-mass structural model (no base mass) are shown for two values of the fixed-base frequencies on Figures 3 and 4. On Figure 3, the fundamental frequency was equal to 4.06 cps. The fixed-base frequency of the containment vessel was tuned to the input wave frequency of 5.0 cps to obtain results plotted on

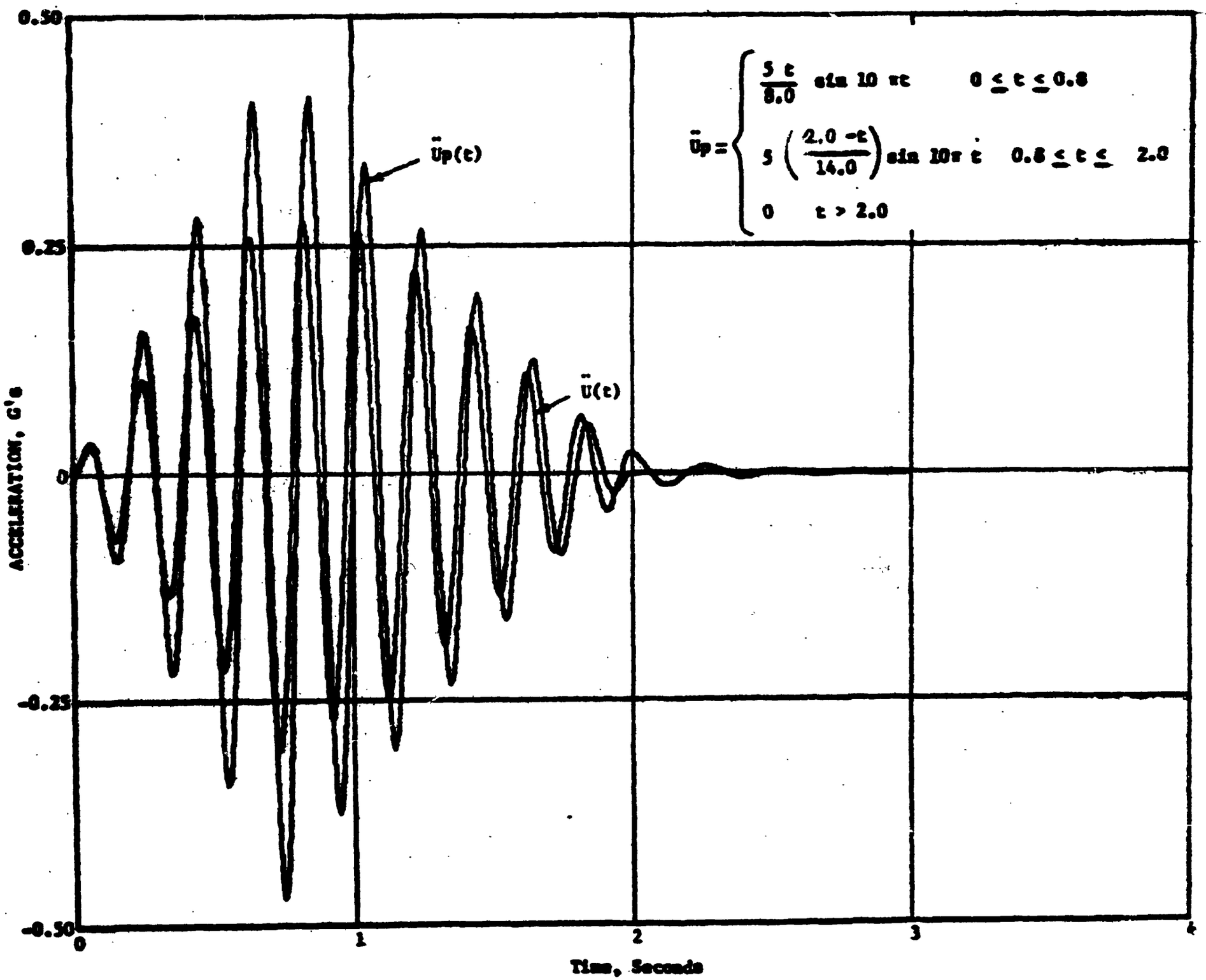

Figure 3 The output acceleration response of a single mass system weighing 475,000 lb-sec^2/ft to a ramp sinusoidal function with a 5 cps is shown. The natural frequency of the system is 4.06 cps and the ground shear wave velocity was taken to be 1000 ft/sec.

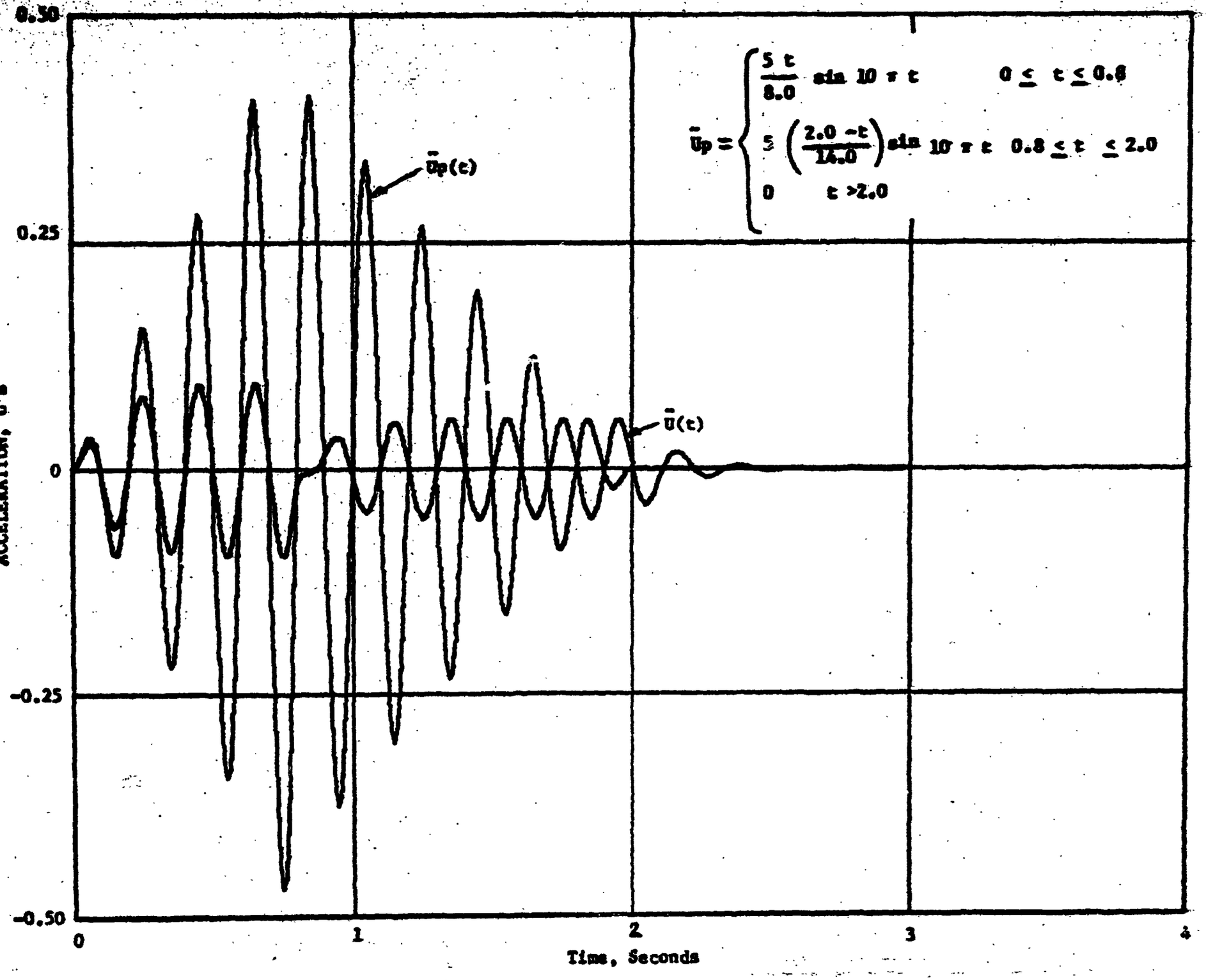

Figure 4 The output acceleration response of a single mass system weighing 475,000 lb-sec^2/ft to a ramp sinusoidal function with a 5 cps is shown. The natural frequency of the system is 5.0 cps and the ground shear wave velocity was taken to be 1000 ft/sec.

Figure 4. It should be noted that the motion at the base of the structure was out-of-phase with the input motion in this calculation. Very similar results were obtained with equation (9) in which a containment vessel-mass-plus-base-mass structural model was subjected to this ideal motion.

Response spectra determined from the calculated foundation motion are compared to the free-field response spectra on Figures 5 and 6 for the containment-vessel only model and the containment-vessel-plus-base-mass model respectively. Only the response spectra at the fixed-base frequencies of the structure are plotted. Thus the results of 6 different calculations are presented on each graph. Calculations were made at fixed-base frequencies of 4.06 cps and 5.0 cps for ground shear wave velocities of 500 ft/sec, 1000 ft/sec and 2000 ft/sec.

Using either mathematical model, it was found that the largest interaction effects occurred when the structure was tuned to the input wave frequency. Furthermore, as seen by comparing Figures 5 and 6, the influence of the large base mass on the accelerations spectrum response at the fixed base frequencies is negligible.

Additional parametric studies were based on the east-west acceleration recorded at Golden Gate Park during the March 1957 San Francisco earthquake (Figure 7). Output acceleration calculated at the base of the containment-vessel only model is shown on Figure 8. For the containment-vessel-plus-base-mass model, the output acceleration is plotted on Figure 9. In both of these cases, the fixed-base frequency of the structure is 4.06 cps and the soil shear wave velocity is 1000 ft/sec. The effect of the base mass on the output acceleration is to reduce the sharp peaks in the acceleration. As a result, the high frequency

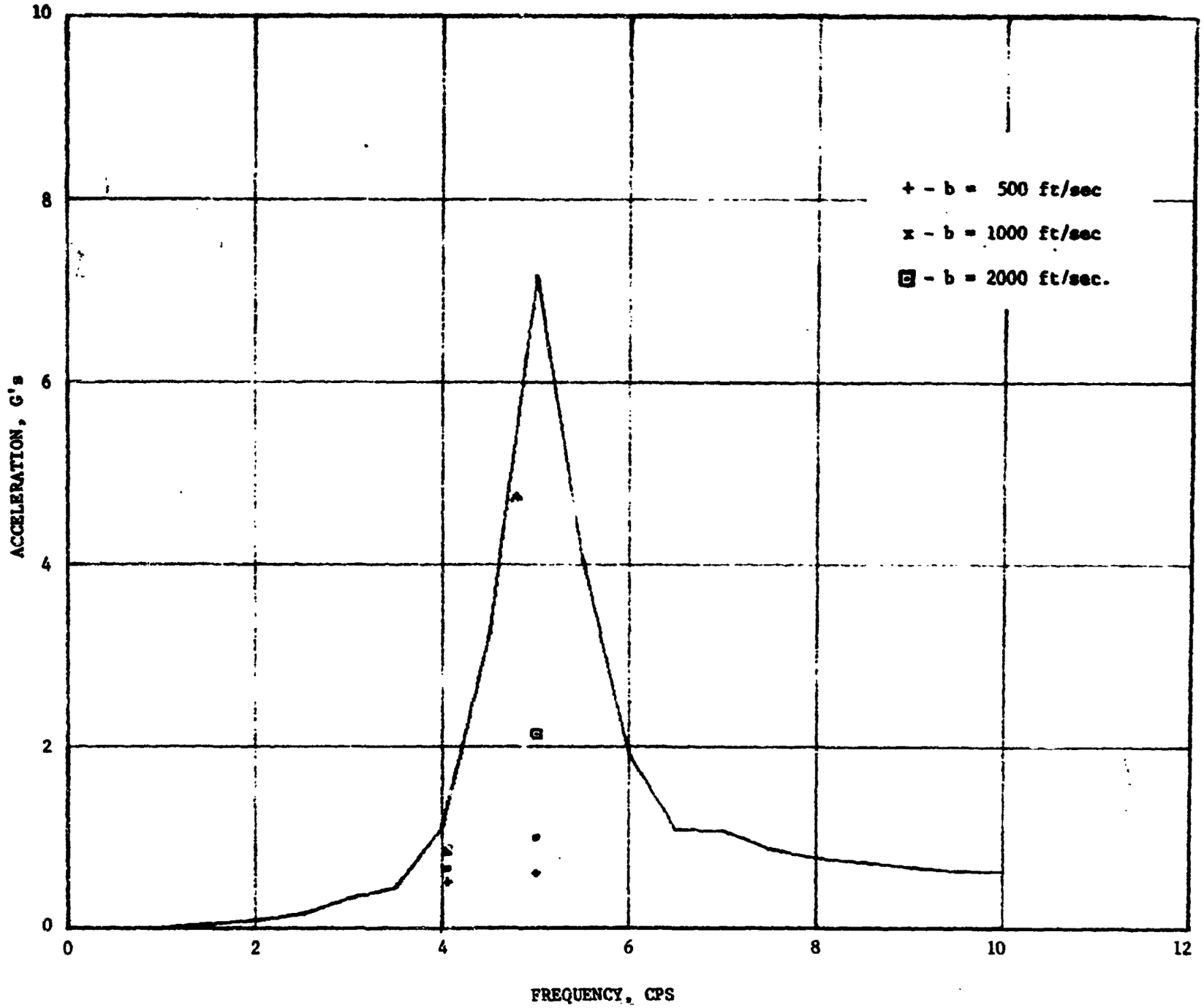

Figure 5 The acceleration response spectrum for the input sinusoidal ramp function is shown as a solid line. The output acceleration response spectra are shown at the fixed base frequencies of 4.06 cps and 5 cps of a one mass system (475,000 $\frac{\text{lb-sec}^2}{\text{ft}}$) without a base mass for three soil shear wave velocities (500 ft/sec., 1000 ft/sec., and 2000 ft/sec.). Large interaction effects can be observed when the natural frequency of the structure is equal to the input wave frequency of 5.0 cps.

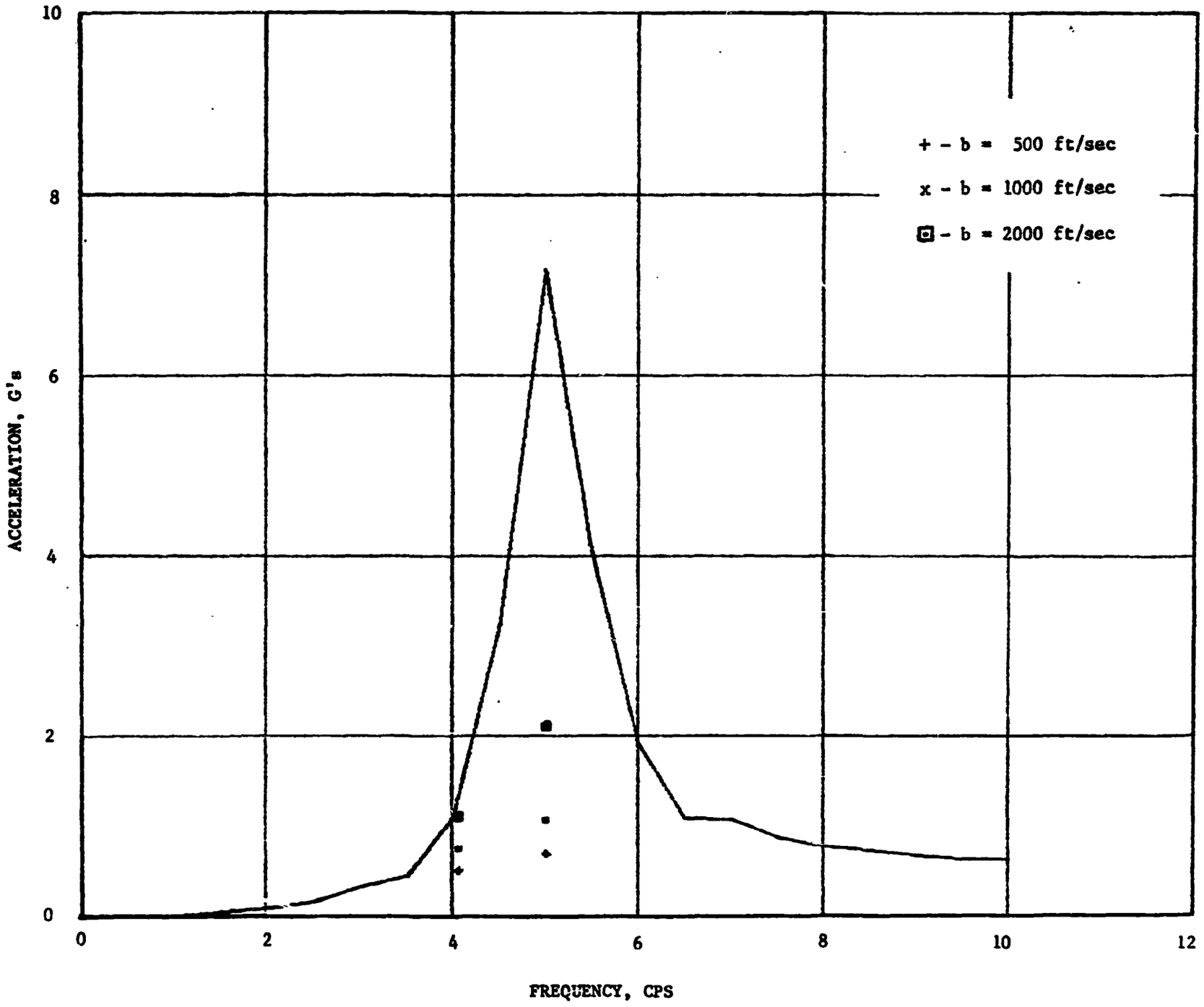

Figure 6 The acceleration response spectrum for the input sinusoidal ramp function is shown as a solid line. The output acceleration response spectra are shown at the fixed base frequencies of 4.06 cps and 5 cps of a system with a base mass (2,400,000 $\frac{\text{lb-sec}^2}{\text{ft}}$) and a single dynamic mass (475,000 $\frac{\text{lb-sec}^2}{\text{ft}}$) for three soil shear wave velocities (500 ft/sec., 1000 ft/sec., and 2000 ft/sec.). Large interaction effects can be observed when the natural frequency of the structure is equal to the input wave frequency of 5.0 cps.

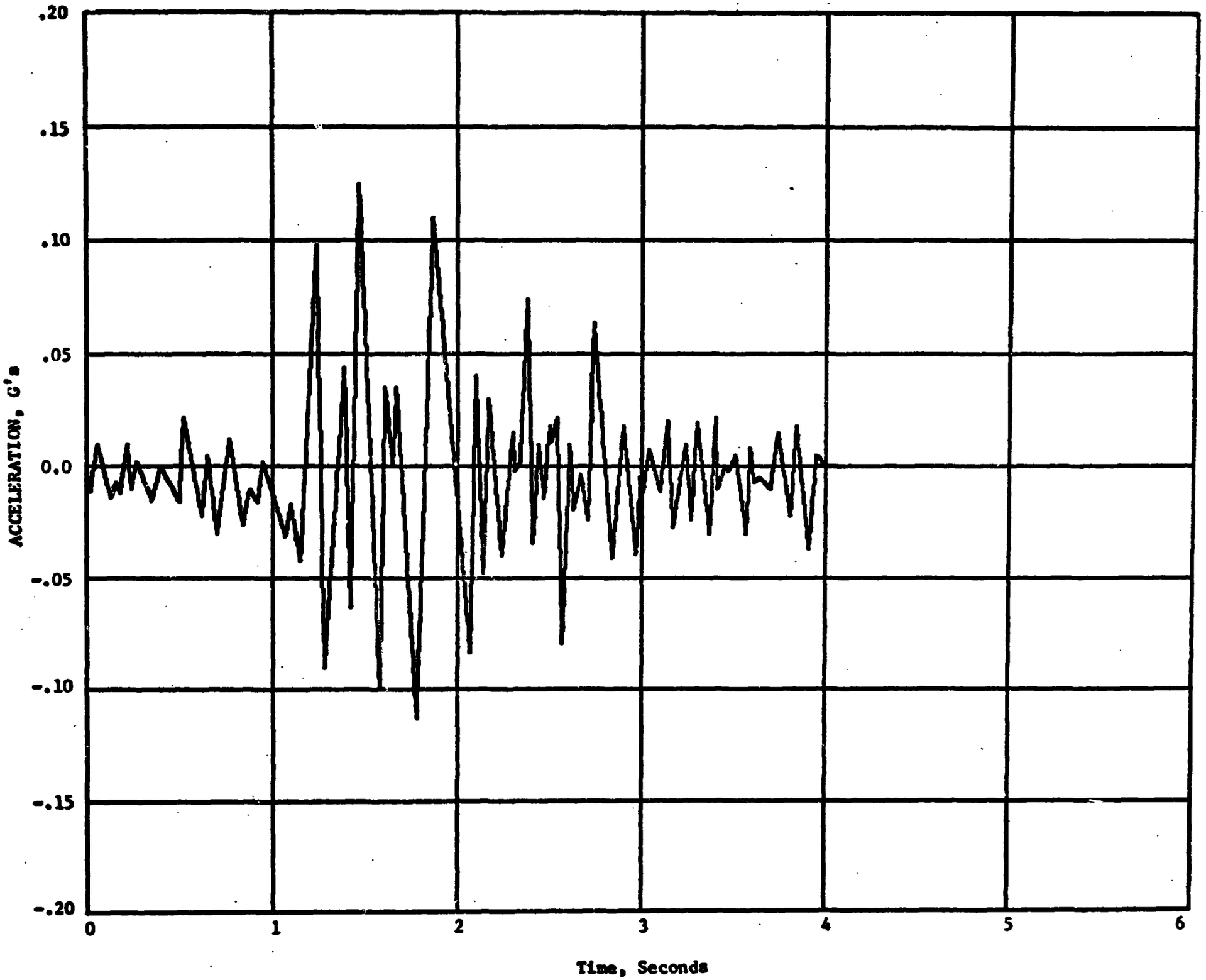

Figure 7 East-west ground acceleration recorded at Golden Gate Park during the March, 1957 San Francisco earthquake.

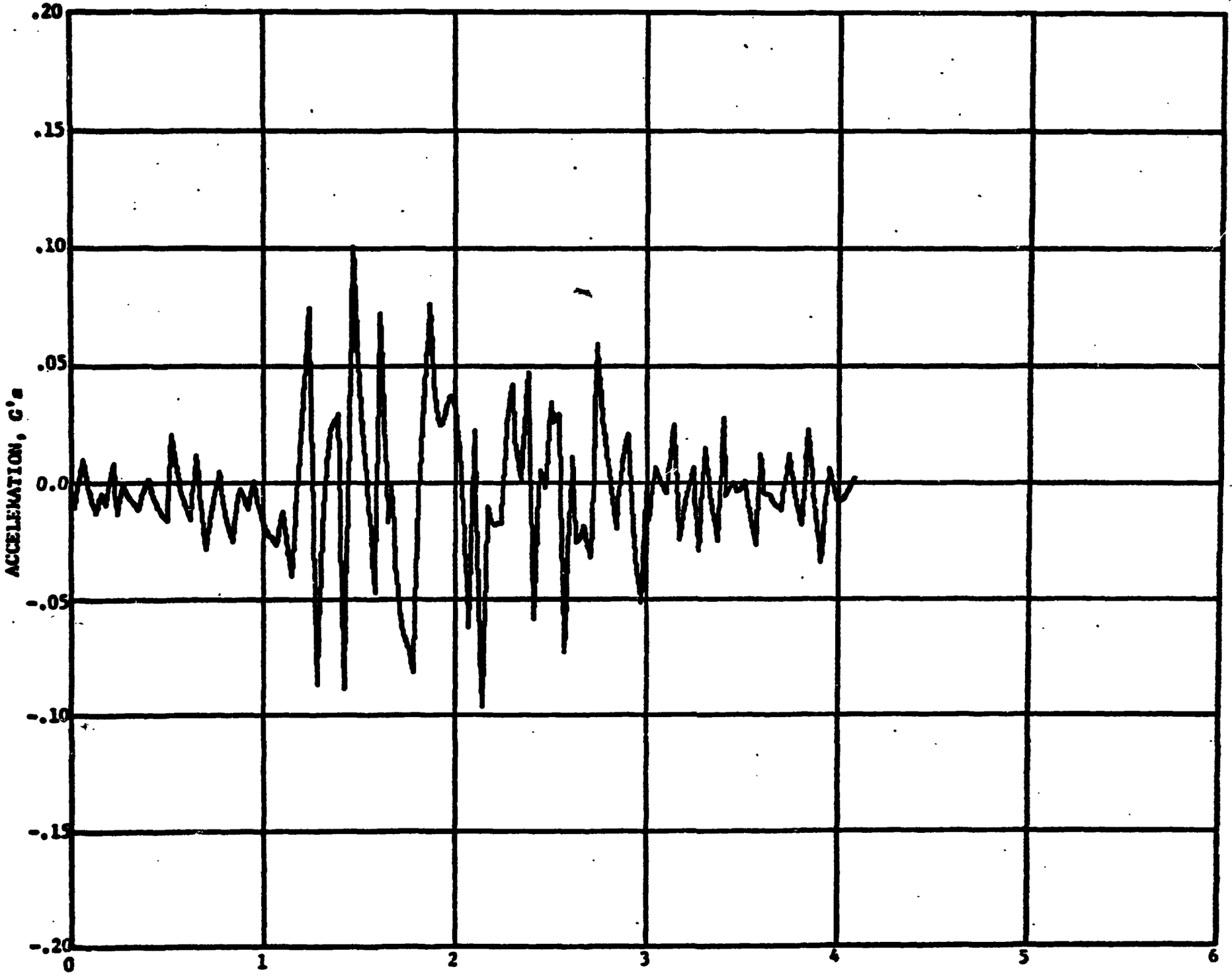

Figure 8 The output acceleration response of a single mass system weighing 475,000 lb-sec^2/ft with a fixed-base frequency of 4.06 cps and a shear wave velocity of 1000 ft/sec. subjected to the Golden Gate east-west ground motion.

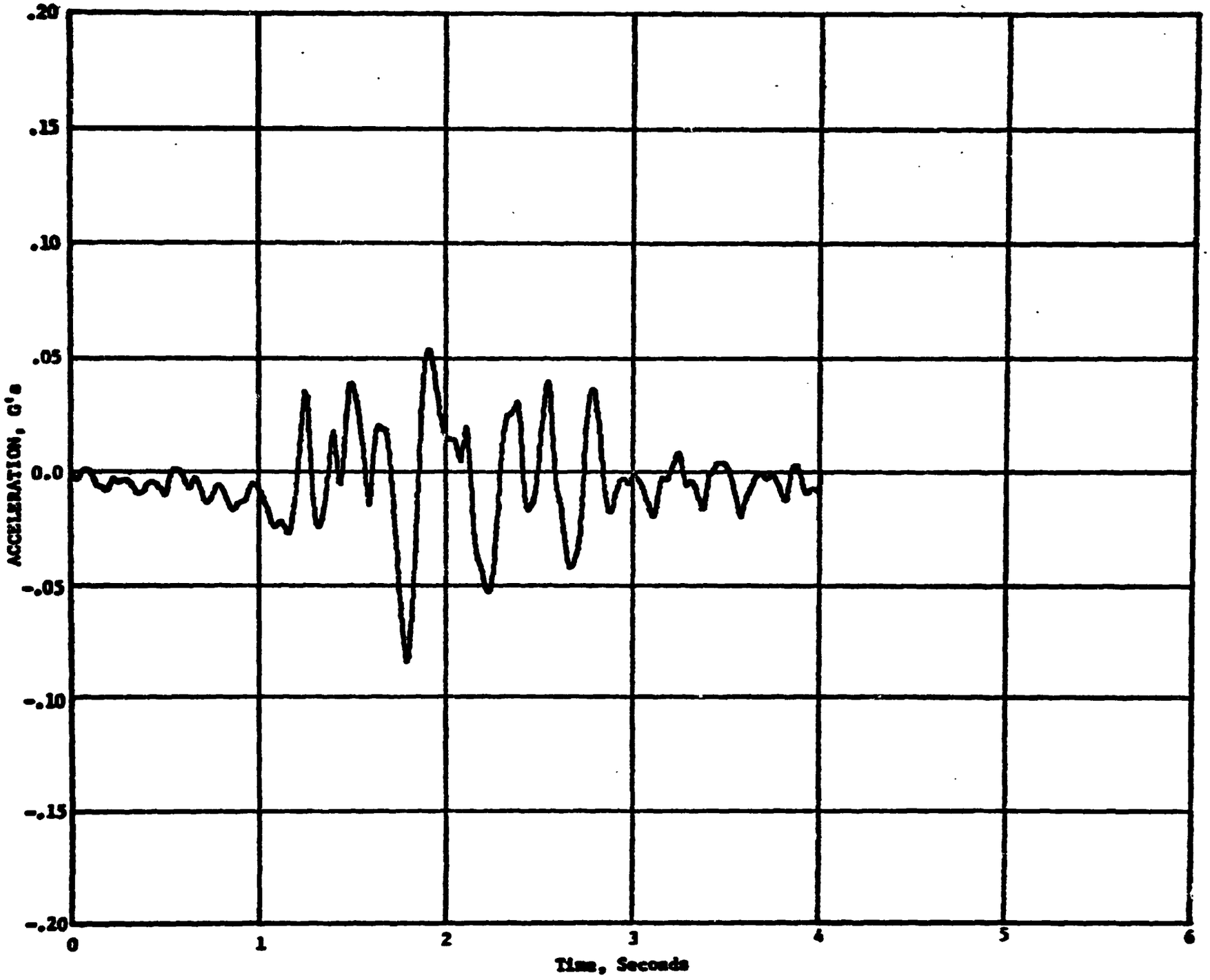

Figure 9 The output acceleration response of a two-man system subjected to the Golden Gate east-west ground motion. The fixed-base frequency of the system is 4.06 and the soil shear wave velocity is 1000 ft/sec.

portion of the response spectrum is reduced. However, at the fixed-base frequency of the structure, the effect of the large base mass on the acceleration response spectrum is not significant (Table I). In fact, the acceleration response spectra was increased slightly by the addition of the large base mass.

The effect of structure frequency on the spectrum response is illustrated on the next three graphs (Figures 10, 11 and 12). The fixed-base frequency of the structure is designated as f_n on these graphs. In all cases, the soil shear wave velocity is 1000 ft/sec. Changes in the entire response spectrum caused by the variation in the fixed-base frequency can be observed. Seismic shock loads on the containment vessel can be determined from these response curves at the fixed-base frequencies of the structure. Thus, if the frequency is 4.06 cps, the loading would be 0.25 g's (Figure 10). If the frequency is 4.44 cps and 5.20 cps the loading would be 0.23 g's and 0.16 g's respectively. However, the spectrum response of the free-field motion is 0.59 g's, 0.84 g's and 0.36 g's for frequencies of 4.06 cps, 4.44 cps and 5.2 cps respectively. Therefore, the interaction effects tend to smooth out large variations in the acceleration spectrum response of the free-field motion. Results with this same two-mass structural model were also obtained for soil shear wave velocities of 500 ft/sec and 2000 ft/sec. Output acceleration spectra are compared to the free-field input spectra on Table II.

The reduction ratio, which is defined as the output acceleration spectrum at the structure frequency divided by the free-field input acceleration spectrum

TABLE I

COMPARISON OF ACCELERATION SPECTRA FOR SYSTEMS SUBJECTED TO EARTHQUAKE MOTION

Structure Description	Shear Wave Velocity Ft./sec.	Fixed-Base Frequency 4.06 cps	
		g's	% Reduction
Free Field Motion	---	0.59	-
Containment-Vessel Mass with No Base Mass	500	0.15	74.5%
	1000	0.19	68.0%
	2000	0.30	49.2%
Base Mass and Containment-Vessel Mass	500	0.16	73.0%
	1000	0.25	57.6%
	2000	0.38	35.6%

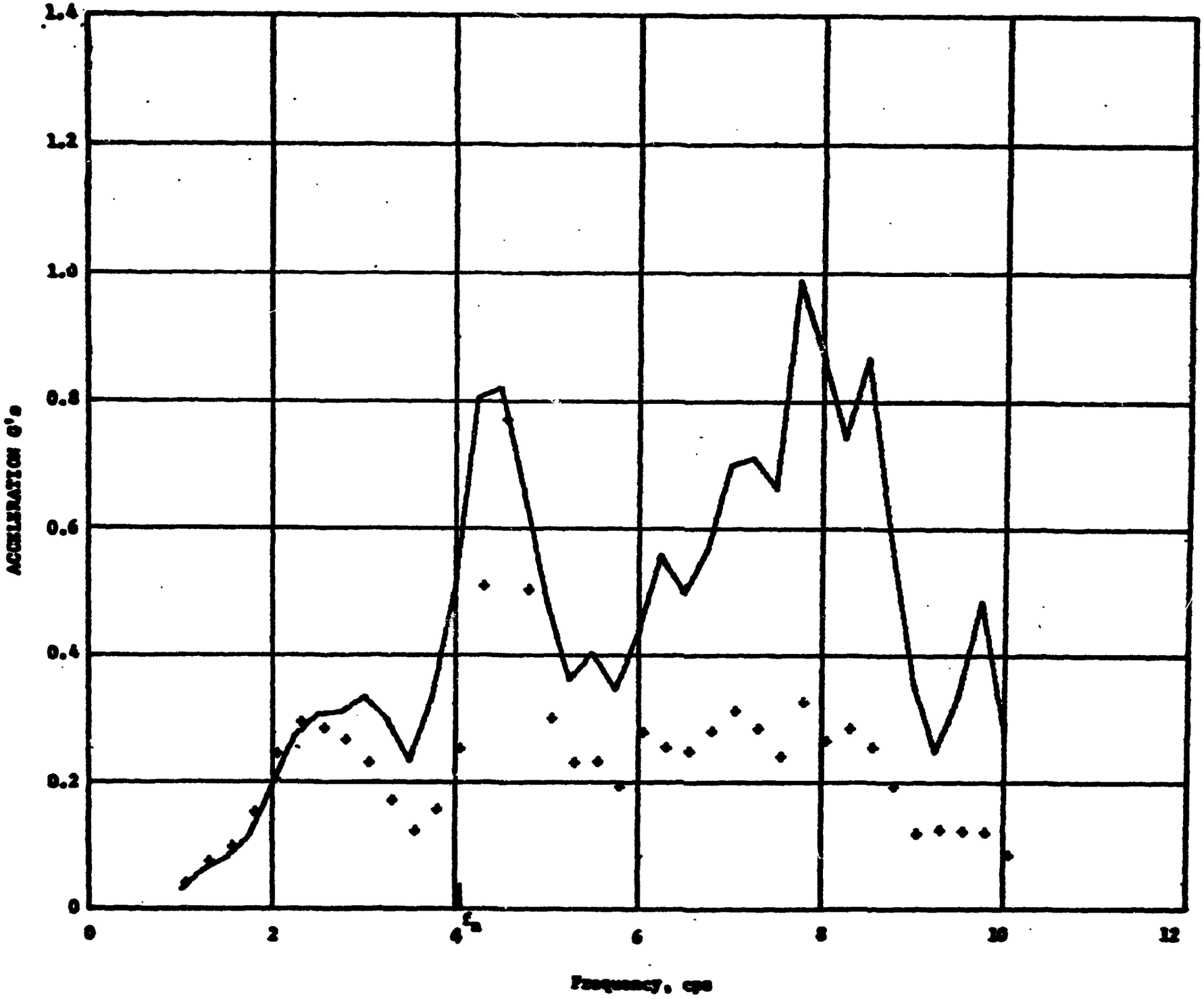

Figure 10 The acceleration spectra of the input Golden Gate east-west ground motion is shown as a solid line. Output spectra calculated from the foundation motion of a containment-vessel-plus-base-mass model with a fixed-base frequency of 4.06 cps are also plotted. The soil shear wave velocity is 1000 ft/sec.

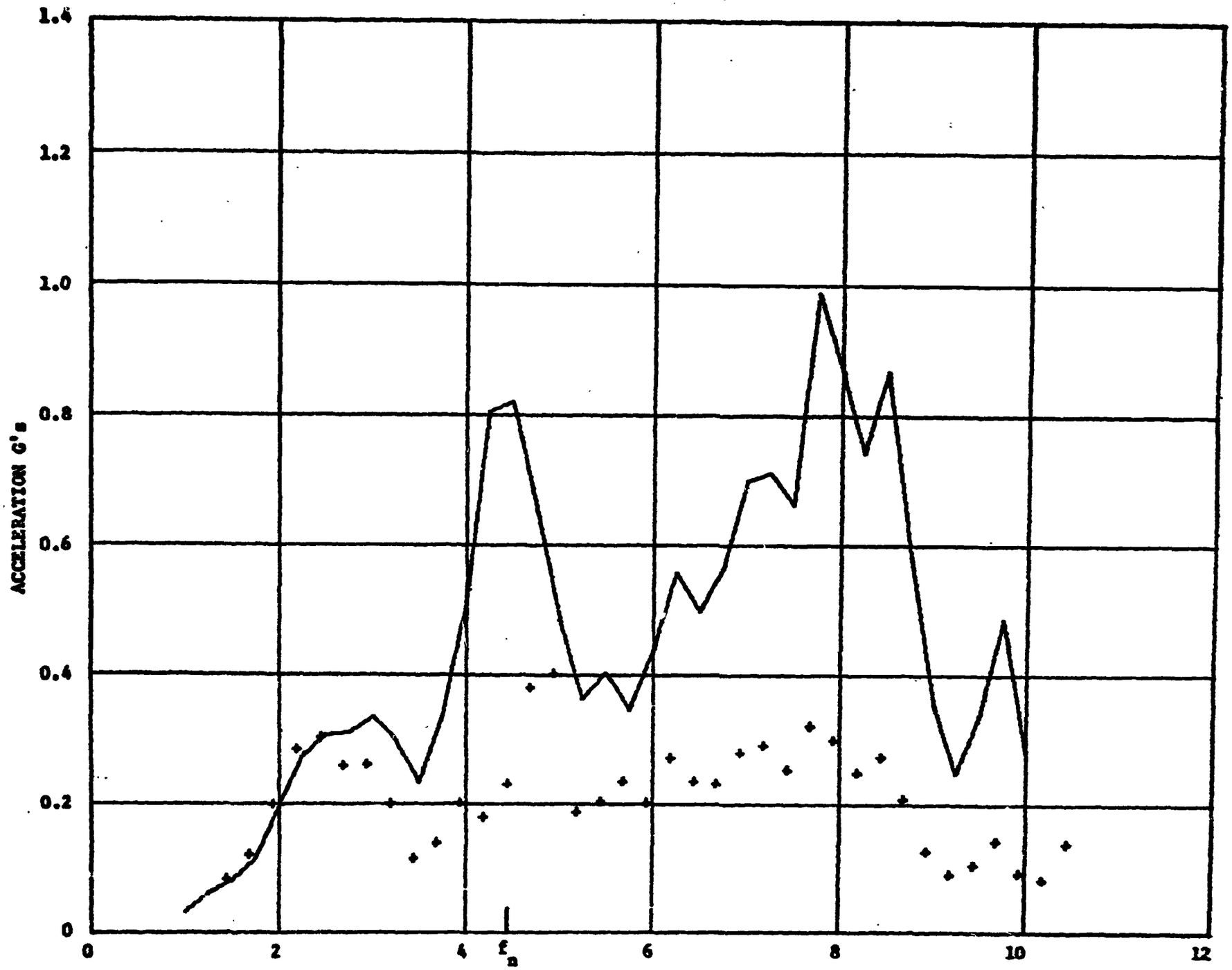

Figure 11 The acceleration spectra of the input Golden Gate east-west ground motion is shown as a solid line. Output spectra calculated from the foundation motion of a containment-vessel-plus-base-mass model with a fixed-base frequency of 4.44 cps are also plotted. The soil shear wave velocity is 1000 ft/sec.

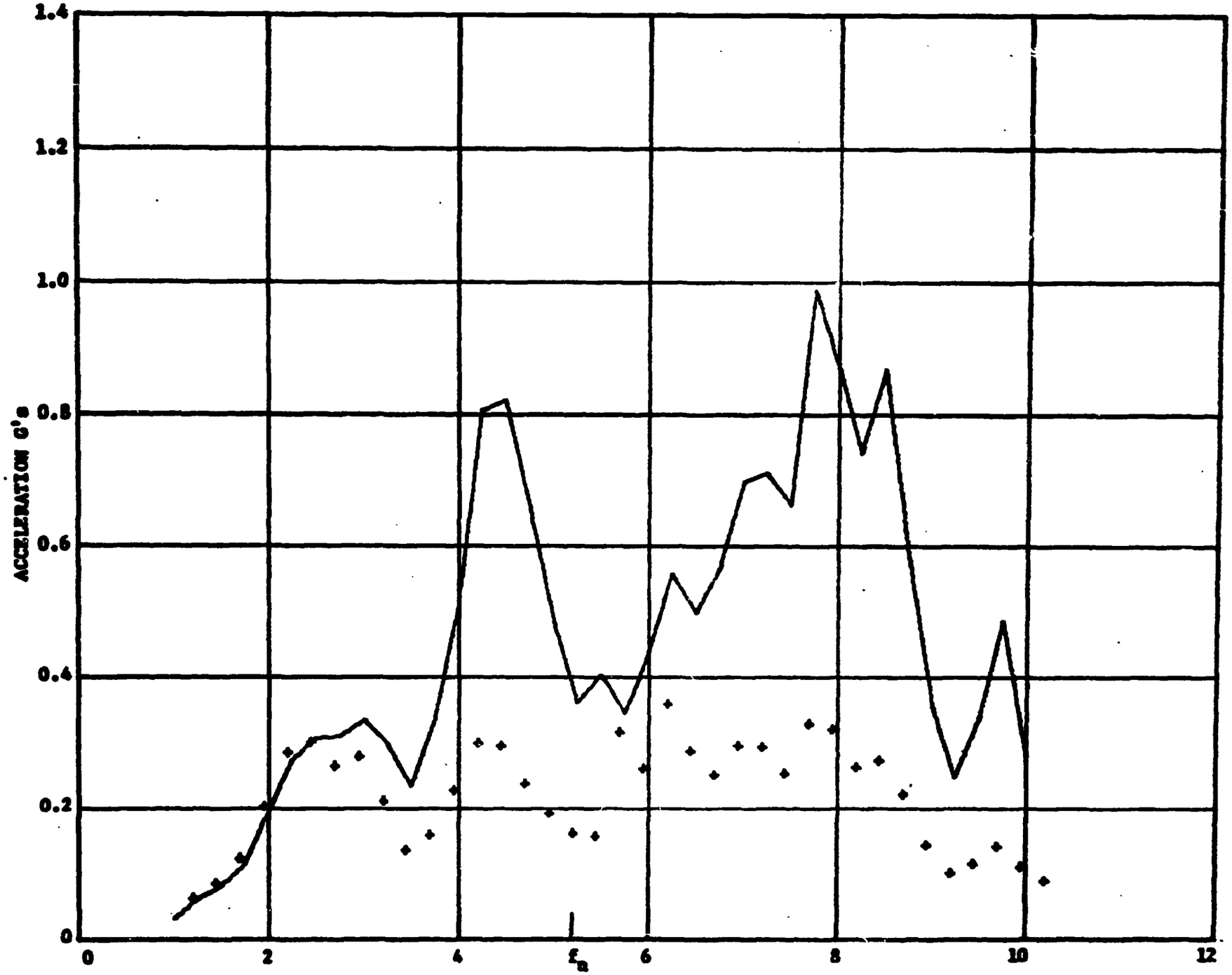

Figure 12 The acceleration spectra of the input Golden Gast east-west ground motion is shown as a solid line. Output spectra calculated from the foundation motion of a containment-vessel-plus-base-mass model with a fixed-base frequency of 75.2 cps are also plotted. The soil shear wave velocity is 1000 ft/sec.

TABLE II

ACCELERATION SPECTRA FOR THE TWO-MASS STRUCTURAL MODEL SUBJECTED TO THE EARTHQUAKE INPUT

Structure Description*	Shear Wave Velocity Ft./sec.	Fixed-Base Frequency					
		4.06 cps		4.44 cps		5.20 cps	
		g's	% Reduction	g's	% Reduction	g's	% Reduction
Free Field Motion	---	0.59		0.84		0.36	
Base Mass and Containment-Vessel Mass	500	0.16	73.0%	0.13	84.5%	0.08	77.8%
	1000	0.25	57.6%	0.23	72.6%	0.16	55.5%
	2000	0.38	35.6%	0.42	50.0%	0.34	5.50%

*The containment-vessel mass is 475,000 $\frac{\text{lb-sec}^2}{\text{ft}}$ and the base mass is 2,400,000 $\frac{\text{lb-sec}^2}{\text{ft}}$. Acceleration spectra are given in g's and the percentage reduction is obtained by dividing the free-field acceleration spectra into the output acceleration spectra and multiplying by 100.

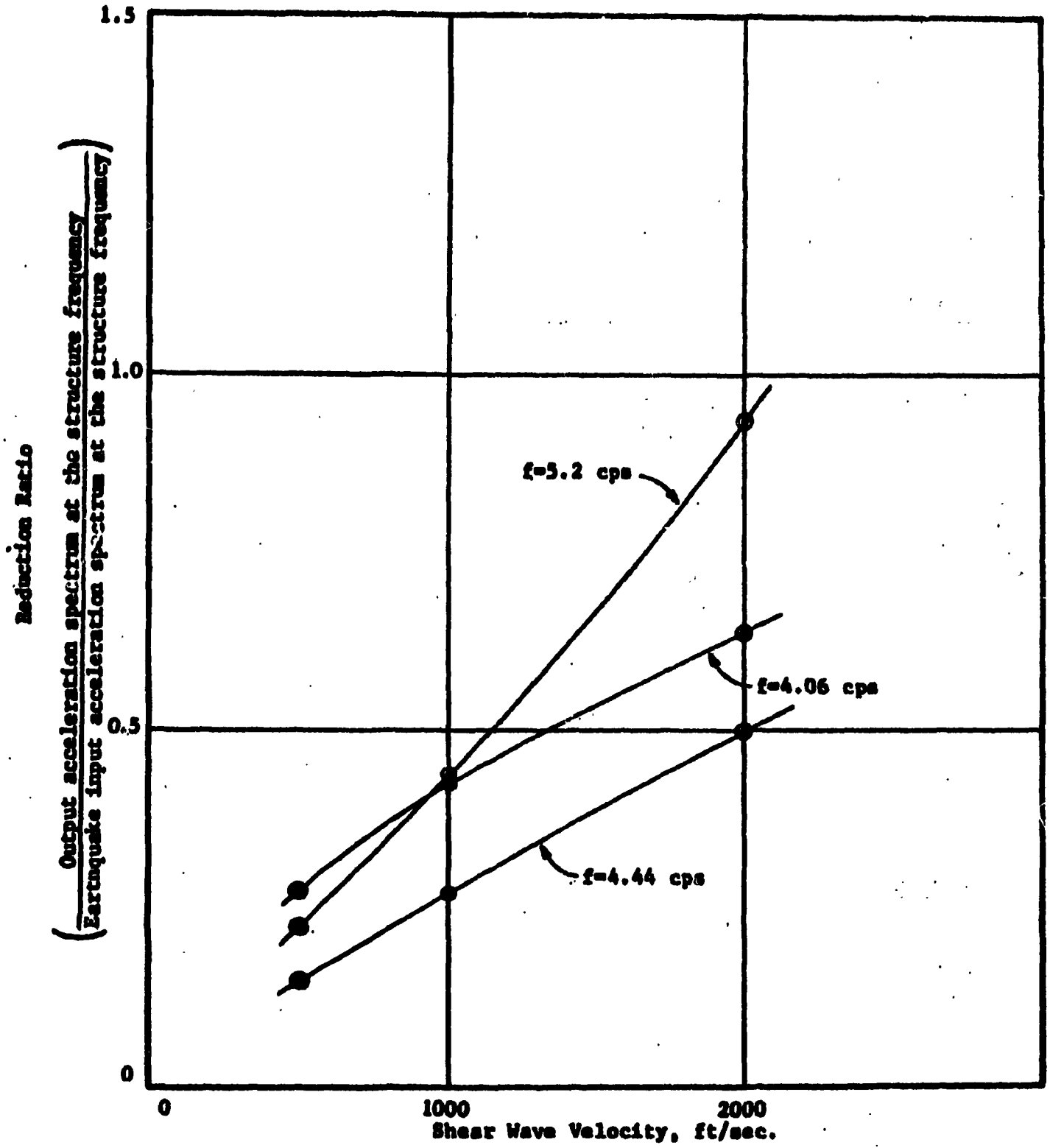

Figure 13 The ratio of the acceleration response spectrum of the base motion to the acceleration response spectrum of the earthquake free-field motion are plotted versus the soil shear wave velocity for the containment-vessel mass with base mass model. Results from three fixed-base frequencies (4.06 cps, 4.44 cps and 5.2 cps) are presented. These curves show that the ratio depends upon both the fixed-base frequency and soil stiffness.

at the structure frequency, is plotted as a function of soil stiffness on Figure 13. As indicated by this graph, the significance of interaction effects depends both on soil stiffness and structure frequency.

Finite Element Studies

A finite element stress wave propagation program, SLAM, was employed by IIT Research Institute to study soil-structure interaction effects. For this study, the SLAM program was modified so that an N-mass structure could be fixed to a number of specified node points in a finite element grid which represents the soil. Rigid body motion can be specified for the node points fixed to the N-mass structure.

In order to verify this modification of the program, interaction effects calculated from a one-dimensional bar were compared to analytical results presented in Reference 9. Agreement between the two methods of analysis is good (8). SLAM Code results are also compared to anaylytical computations of Baron et. al. (10) and Yoshihara et. al. (11) for a two-dimensional embedded cylinder.

After verification of the program modification, three interaction problems designated as Surface Model I, Surface Model II and the Embedded Model were studied. All problems were run before the nonreflecting boundary technique was incorporated into the SLAM Code. Thus, in order to eliminate unwanted reflections from the boundaries, a very large finite element mesh was employed which was approximately 2900 ft. long by 2200 feet deep. Furthermore, in order to keep the running time on the machine reasonable, the mesh size was changed throughout the grid. A fine mesh was used under the base of the structure and a course grid away from the structure. The finite element mesh for the surface cases is shown on Figure 14. The modification of this soil model for the embedded case is shown on Figure 15.

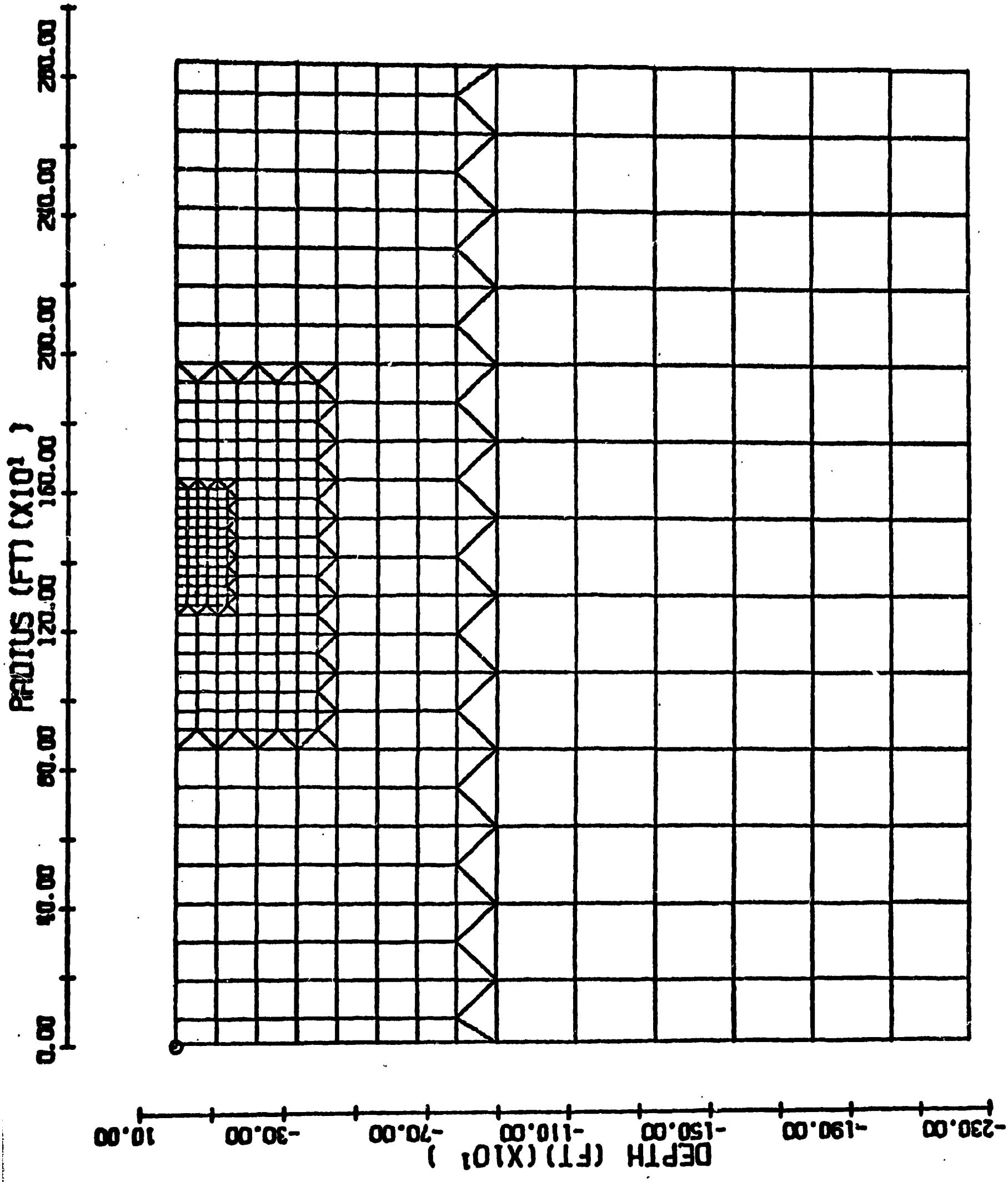

Figure 14 SLAM soil model for surface reactor problems

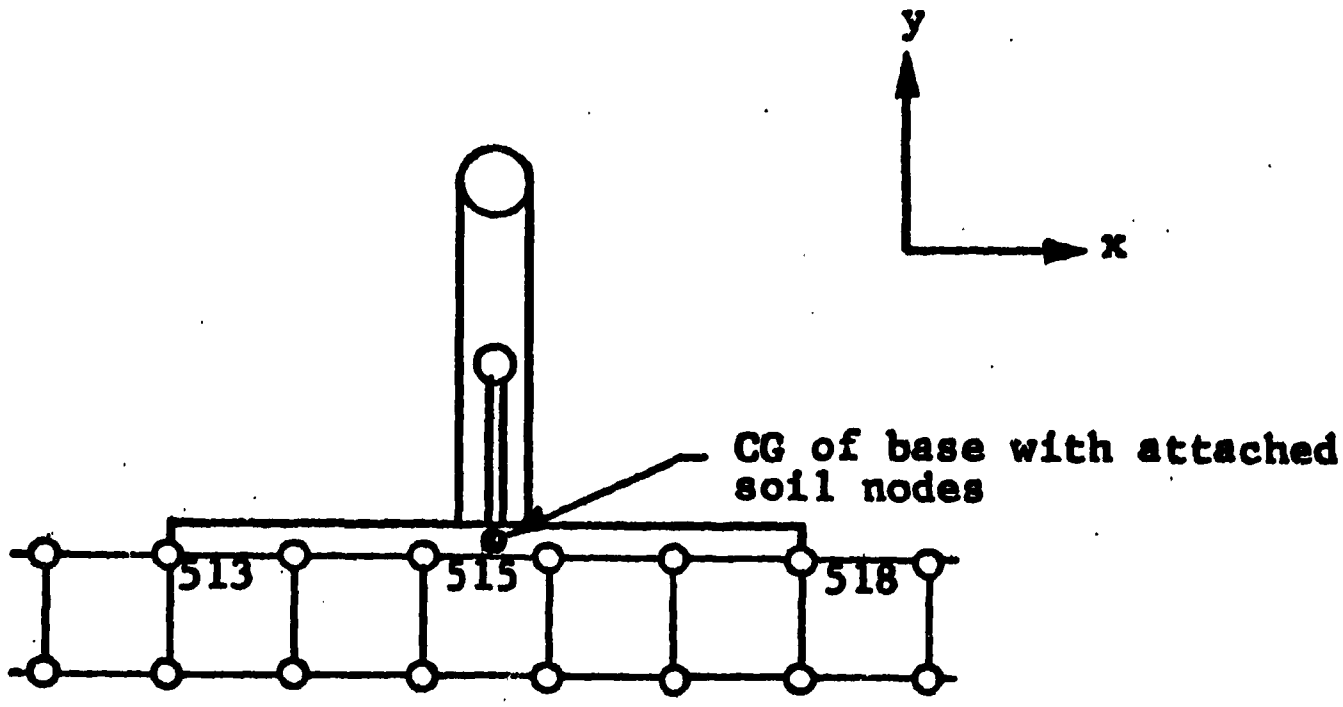

(a) Surface Model

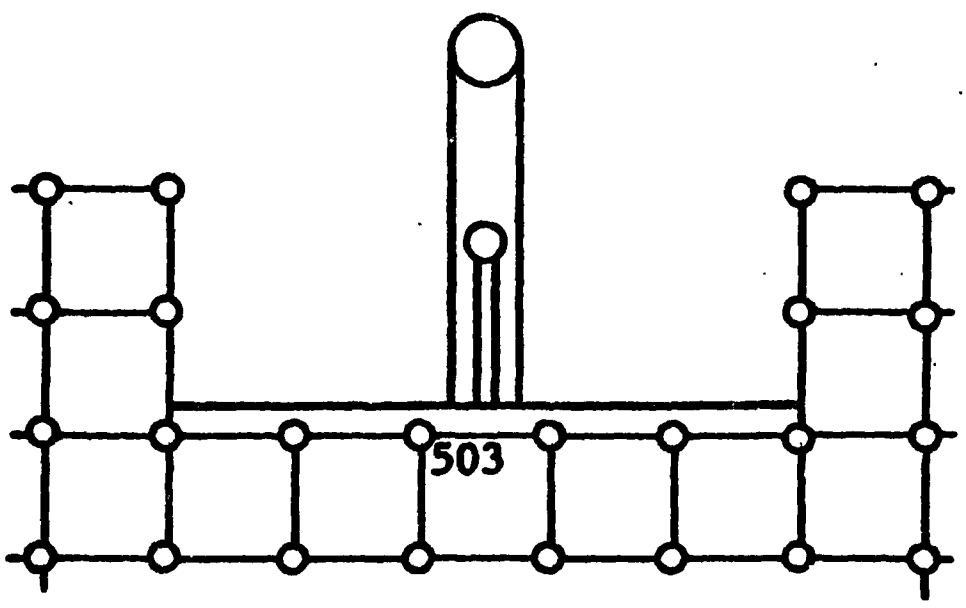

(b) Embedded Model

Figure 15 **Attachment of reactor models to soil mesh**

Soil properties used in the mesh for all calculations are as follows:

Weight Density	=	95 lb/ft^3
Elastic Modulus	=	33,000 psi
Poisson's Ratio	=	0.25
Shear Wave Velocity	=	802 fps

Structure properties were based on the three mass model shown on Figure 2. Input values were modified to account for the plane strain finite element soil model as follows:

M_o	=	2400/110 = 21.8 K-Sec 2/ft.
m_1	=	475/110 * 4.32 K-Sec 2/ft.
m_2	=	310/110 = 2.82 K-Sec 1 ft.
k_2	=	$0.13 \times 10^6/100 = 0.282 \times 10^4$ K/ft$^2_2$
k_3	=	$0.30 \times 10^6/110 = 0.272 \times 10^4$ K/ft^2
I_1	=	$20 \times 10^6/110 = 18.2 \times 10^4$ K Sec^2

For Surface Model II all of the properties remained the same except that k_2 was doubled to a value of 0.544×10^4 K/ft^2

The reactor model was centrally located above the area of the smallest finite element grid shown on Figure 14. The base was attached to six nodes as shown in Figure 15a. There was no rigid body motion between these nodes. For the embedded case, the reactor was located at the same horizontal location in the mesh as for the two surface cases but it was buried 56 feet and attached to the soil (Figure 15b). Furthermore, the vertical sides of the reactor below the ground level were assumed to be rigid, massless, extensions of the rigid reactor base.

Loading of the soil-structure configuration was introduced by forcing the boundary nodes on the left-hand boundary of the soil mesh with specified horizontal motion. The specified motion is identical to that used in the analytical studies and given by equation (10). In all cases this seismic pulse of 2 second duration at the reactor location was used to avoid reflections of of waves from the boundaries. The magnitude of input motion was assumed to be uniform with depth along the boundary from the surface to 784 feet in depth. From 784 feet to 1120 feet, a linear variation in amplitude to zero at 1120 feet was assumed. Below 1120 feet there was no input motion on the left-hand boundary. The top and right-hand boundaries were free and the bottom boundary was fixed.

In a computation without a reactor model present, the free-field motions for the soil mesh at the reactor location were determined and graphed on Figure 16. Motions calculated at node 515, which is located just to the left of center (Figure 15a) are presented.

Even though only horizontal motion was used as input to the finite element mesh both vertical and horizontal motions were present at node 515. The vertical motion is caused primarily by the presence of the free surface. Also, the shape of the horizontal wave is altered significantly from the input motion. This change is believed to be caused by the large mesh size in the soil model, changes in the mesh size and generation of the surface wave. Even though this distortion of the input wave occurred, effects of soil-structure interaction can be adequately evaluated by studying changes in this calculated free-field motion.

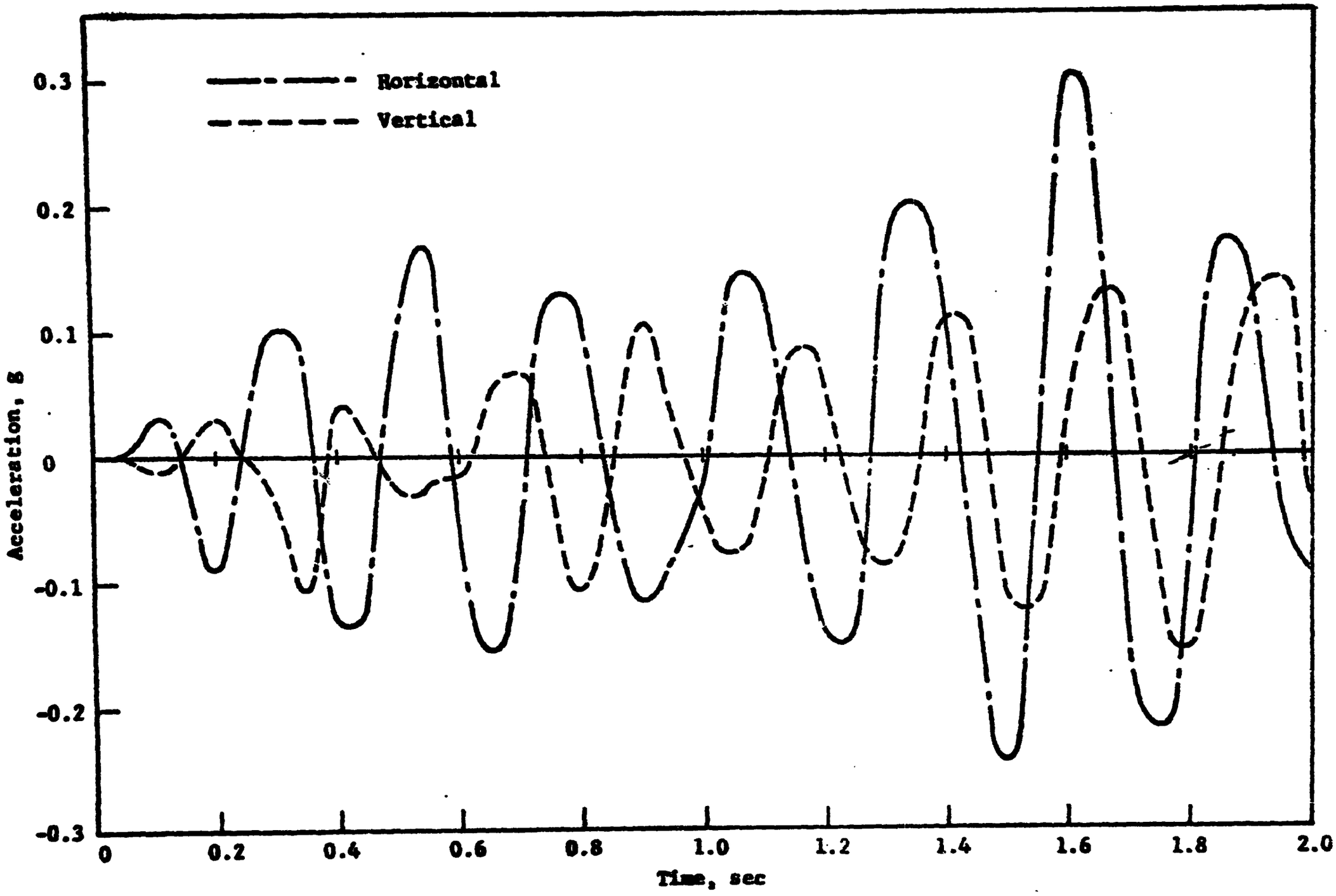

Figure 16 Free Field accelerations at node 515

Horizontal and vertical accelerations calculated at the reactor base at node 515 for Surface Model I and for the Embedded Model are graphed on Figures 17 and 18 respectively. It should be noted that peak accelerations are reduced from a value of approximately 0.31 g's (free-field motion) to approximately 0.10 g's and 0.13 g's for Surface Model I and the Embedded Model, respectively. Changes in the response spectra from free-field values are presented on Tables III and IV for the horizontal and vertical directions. At the horizontal fixed-base frequencies of the containment structure and internal structure, the changes in the acceleration response spectra are listed in Table V. The free-field acceleration response spectra were reduced from a factor of approximately 2 to 5.

Rocking motion of the rigid base was also studied. In Reference (8), results are presented in terms of a rotational spectrum response. The peak acceleration possible from the rocking motion alone is approximately the same magnitude as the contribution of the horizontal foundation motion. These results are summarized in Table VI. Subsequent work, presented below, shows that the phase relationship between the translational motion of the base and the rotation of the base must be considered.

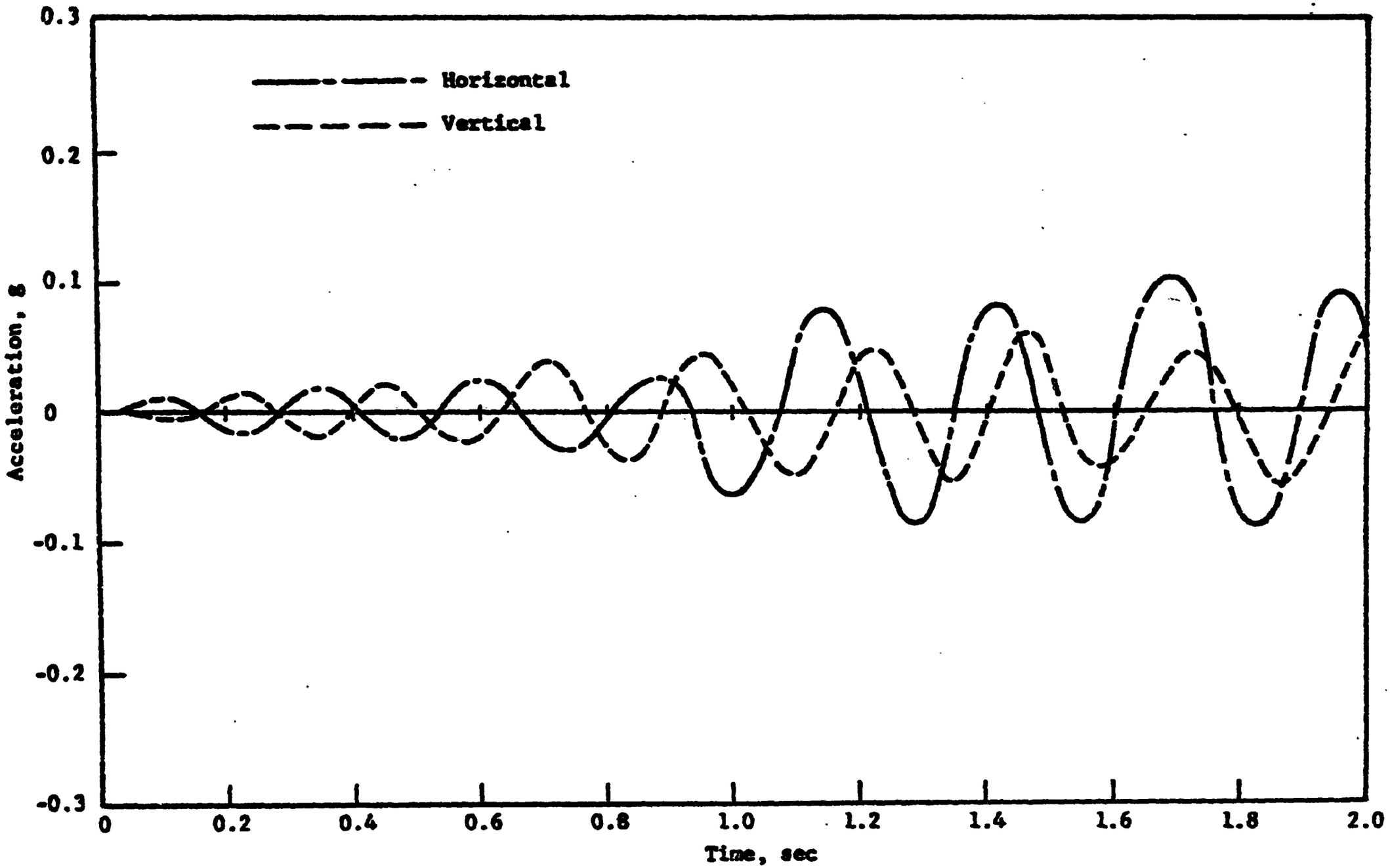

Figure 17 Accelerations of reactor base at node 515, Surface Model I

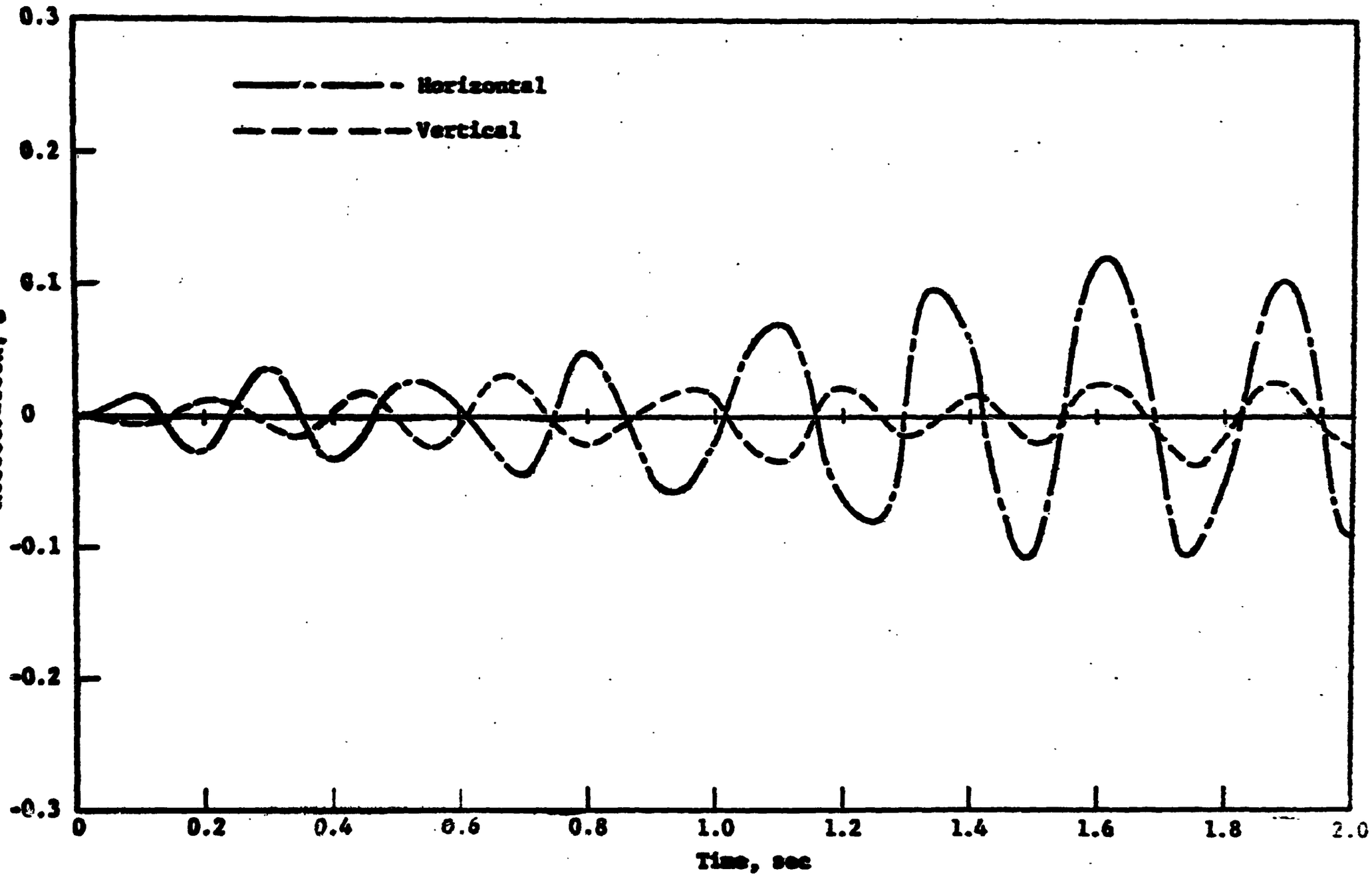

Figure 18 **Accelerations of reactor base at node 503, Embedded Model**

TABLE III

HORIZONTAL SPECTRA ACCELERATION

Frequency cps	Horizontal Acceleration Spectra Values, g				Spectra Acceleration Ratio, β (Structure Accel. / Free Field Accel.)		
	Free Field	Base of Structure					
		Surface Model I	Surface Model II	Embedded Model	Surface Model I	Surface Model II	Embedded Model
1.0	0.0296	0.0210	0.0215	0.0217	0.709	0.726	0.733
1.5	0.0765	0.0456	0.0464	0.0417	0.596	0.607	0.545
2.0	0.157	0.125	0.127	0.1025	0.796	0.809	0.653
2.5	0.279	0.176	0.182	0.153	0.631	0.652	0.548
3.0	0.690	0.287	0.296	0.267	0.416	0.429	0.387
4.0	2.53	0.961	0.988	1.22	0.380	0.391	0.482
5.0	1.48	0.260	0.481	0.332	0.176	0.325	0.224
6.0	0.773	0.204	0.204	0.332	0.264	0.264	0.431
8.0	0.562	0.145	0.164	0.194	0.258	0.292	0.345

TABLE IV

VERTICAL SPECTRA ACCELERATION

Frequency cps	Vertical Acceleration Spectra Values, g				Spectra Acceleration Ratio, β (Structure Accel. / Free Field Accel.)		
	Free Field	Base of Structure					
		Surface Model I	Surface Model II	Embedded Model	Surface Model I	Surface Model II	Embedded Model
1.0	0.0363	0.0142	0.0143	0.00948	0.391	0.394	0.261
1.5	0.0866	0.0371	0.0375	0.0269	0.428	0.433	0.311
2.0	0.111	0.0409	0.0410	0.0249	0.368	0.369	0.224
2.5	0.209	0.0813	0.0822	0.0439	0.389	0.393	0.210
3.0	0.463	0.121	0.122	0.166	0.261	0.263	0.359
4.0	2.09	0.907	0.902	0.329	0.434	0.432	0.157
5.0	0.548	0.260	0.275	0.280	0.474	0.502	0.511
6.0	0.565	0.196	0.208	0.106	0.347	0.368	0.188
8.0	0.348	0.0926	0.0964	0.0515	0.266	0.277	0.148

TABLE V

EFFECT OF SOIL-STRUCTURE INTERACTION
ON RESPONSE OF CONTAINMENT AND INTERNAL SUPPORT STRUCTURES

Reactor Model	Lumped Mass	Fixed-Base Frequency of Mass, cps	Horizontal Acceleration Ratio (Structure Accel. / Free Field Accel.)
Surface Model I	Internal Support Structure	5	0.176
	Containment Structure	4	0.380
Surface Model II	Internal Support Structure	7	0.278
	Containment Structure	4	0.391
Embedded Model	Internal Support Structure	5	0.224
	Containment Structure	4	0.482

TABLE VI

EFFECT OF BASE ROCKING

Reactor Model	Lumped Mass	Fixed-Base Frequency of Mass cps	Horizontal Acceleration Spectra Values, g	
			Due to Base Translation Alone	Due to Base Rocking Alone
Surface Model I	Internal Support Structure	5	0.26	0.21
	Containment Structure	4	0.961	1.07
Surface Model II	Internal Support Structure	7	0.184	0.094
	Containment Structure	4	0.988	1.08
Embedded Model	Internal Support Structure	5	0.332	0.148
	Containment Structure	4	1.22	1.02

Comparison of Analyses

A direct comparison was made between SLAM Code results (Surface Model I) and those based on equation (9). Free-field horizontal accelerations calculated at node 515 by the SLAM Code and graphed on Figure 16 were used as input to equation (9). Furthermore, the fixed-base frequencies of the containment structure and internal structure were taken to be 27.5 rad/sec. and 33 rad/sec respectively. These values were based on the eigenvalue problem solved to determine the model properties needed for input to the modified SLAM Code (8). Foundation accelerations of the reactor structure calculated using both methods of analysis are compared on Figure 19 and calculated acceleration spectra are listed on Table VII.

Maximum values of horizontal foundation acceleration calculated from these two methods of analysis are similar in magnitude. However, near 0.6 seconds and 1.7 seconds, the phase relationship of the two solutions differ. There are significant differences between the response spectra near the fixed-base frequencies of 4.0 cps and 5.0 cps. At 4.0 cps, the acceleration spectrum value calculated from SLAM results is greater than the value which is based on equation (9). At 5.0 cps, the value base on equation (9) exceeds the SLAM Code results. At other frequencies, the agreement is satisfactory.

A comparison between results of equation (9) and finite element calculations of Ababian-Jacobsen and Associates has been made (12). However, in this case, agreement between the response spectra was very good. Differences at the fixed-base frequencies of 4 cps and 5 cps, were approximately 1% and 5% respectively.

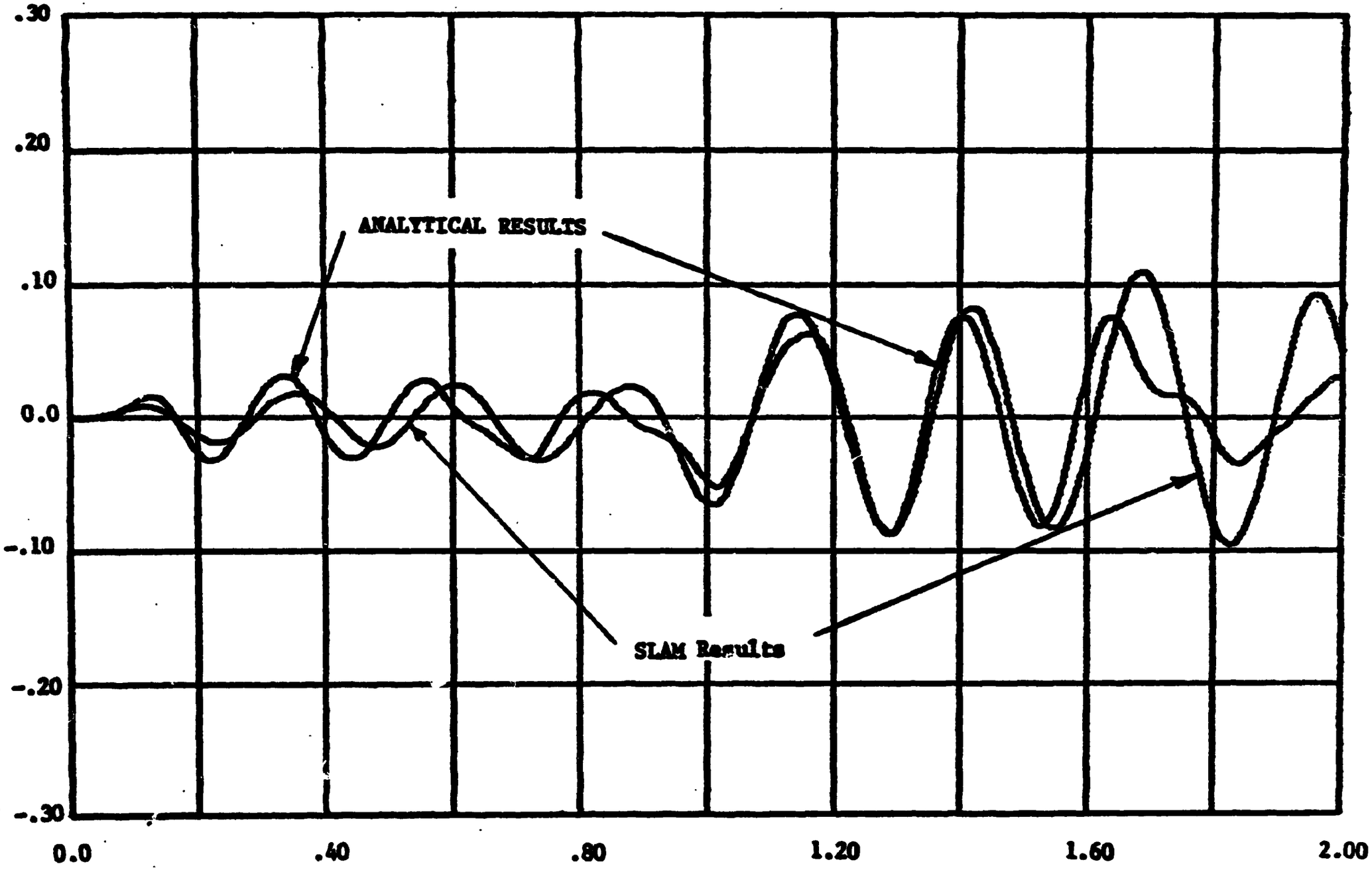

Figure 19 Output accelerations to Surface Model I calculated by IIT Research Institute with the SLAM code are compared to to results from the analytical methods developed at The University of Toledo.

TABLE VII

A COMPARISON OF ACCELERATION RESPONSE SPECTRA

FOR SURFACE MODEL I

Frequency cps	Free Field Acceleration g's	Output Acceleration, g's		Spectra Acceleration Ratio, β	
		U of T	IITRI	U of T	IITRI
1.0	.0297	.0180	.0210	.61	.71
1.5	.0765	.0401	.0456	.52	.60
2.0	.1574	.0850	.125	.54	.79
2.5	.2789	.1186	.176	.42	.63
3.0	.6910	.2342	.287	.34	.42
4.0	2.5360	.6562	.961	.26	.38
5.0	1.4876	.4229	.260	.28	.18
6.0	.7729	.2413	.204	.31	.26
8.0	.5630	.1519	.145	.27	.26

The reason for the discrepancy in the acceleration spectrum response between the SLAM Code and equation (9) is not known. It is speculated that the relatively large mesh size and rocking effects in the SLAM Code caused the differences in response spectrum. However, both methods of analysis show significant reductions on the free-field spectra as shown by the spectra acceleration ratio, β , listed on Table VII.

Rotational Effects

The study of the rotational effects caused by base motion on seismic forces was done with two objectives in mind: to determine the magnitude of accelerations on a structure caused by rotational foundation motion as compared to those caused by lateral foundation motion, and to determine if peak structure accelerations can be estimated by adding accelerations from the rotational spectrum response and lateral spectrum response.

A single lumped mass dynamic system with base rotation can be idealized as shown on Figure 20. The equation of motion can be written as:

$$m\,\ddot{x}(t) + k(x(t) - u(t) - \ell\alpha(t)) = 0 \qquad (11)$$

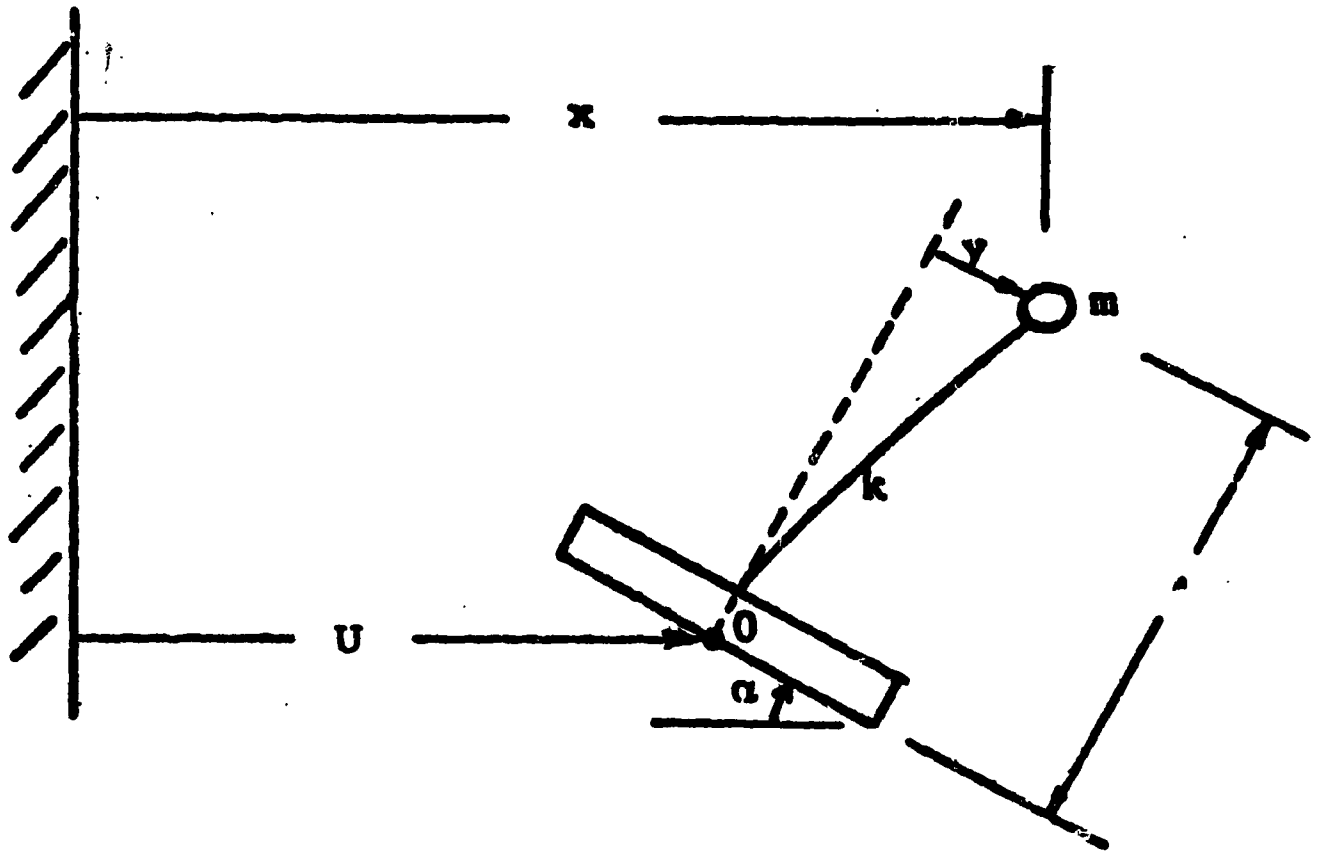

Figure 20 Lumped mass system with foundation rotational motion.

Letting

$$z(t) = x(t) - u(t) - \ell\alpha(t) \tag{12}$$

Then equation (11) becomes

$$\ddot{z}(t) + \omega^2 z(t) = - \ddot{u}(t) - \ell\ddot{\alpha}(t) \tag{13}$$

The solution of equation (12) is

$$z(t) = - \frac{1}{\omega}\int_0^t \ddot{u}(\tau)\sin\,\omega(t-\tau)d\tau - \frac{1}{\omega}\int_0^t \ell\ddot{\alpha}(\tau)\sin\,\omega(t-\tau)d\tau \tag{14}$$

Substituting equations (12) and (14) into (11), the absolute accelerations of the mass, m, can be expressed as:

$$\ddot{x}(t) = \omega\int_0^t \ddot{u}(\tau)\sin\,\omega(t-\tau)d\tau + \omega\int_0^t \ell\ddot{\alpha}(\tau)\sin\,\omega(t-\tau)d\tau \tag{15}$$

Thus, the acceleration of the mass, m, can be expressed as the sum of two integrals. The first integral is the contribution of the horizontal foundation acceleration, $\ddot{u}(t)$, and the second integral is the contribution of the foundation rotational acceleration, $\ddot{\alpha}(t)$. The peak value of the first integral for all time is the horizontal spectrum at the frequency, ω. Similarly, the peak value of the integral, $\omega\int_0^t \ddot{\alpha}(\tau)\sin\,\omega(t-\tau)d\tau$, may be thought of as the rotational spectrum at the frequency, ω, expressed in units of rad/sec^2. By multiplying this rotational spectrum by the height, ℓ, the maximum possible lateral acceleration of the mass, m, caused by base rotation is obtained.

Both the foundation horizontal motion and the foundation rotational motion determined from the three SLAM Calculations are listed as a function of time

in Appendix B of Reference (8). By carrying out the integrations indicated in equation (15) numerically, rotational effects can be studied and compared to lateral accelerations.

Results for the calculation designated a Surface Model II are graphed on Figure 21. In this calculation, the accelerations of the containment vessel mass which is 133' above the foundation are calculated. On the upper plot of the graph the lateral contribution, which is the first integral term in equation (15), is presented. The rocking contribution, which is the second integral term, is shown on the middle plot and the sum of the two terms on the lower graph. Results show that the peak acceleration of the containment vessel mass is much less than either the lateral contribution or rotational spectrum. As a result, maximum forces on the containment vessel can not be estimated accurately from either the lateral spectrum response or rotational spectrum response . The peak acceleration is less than either value. It is evident from the graph that the reason for this reduction is that the lateral motion and rotational motion are out-of-phase with each other.

Similar results were obtained for other calculations which are summarized on Table VIII. Motions of the containment vessel mass (4 cps and 133 feet height) and the internal structure mass (5 cps and 55 feet height*) were studied. In addition, motions at one half of the heights were also studied. In all cases, the peak structure acceleration was less than the sum of the lateral contribution (which is the lateral spectrum value) and rotational contribution (which is the rotational spectrum times the height).

* For Structure Model II, the frequency of the internal structure was increased to 7 cps.

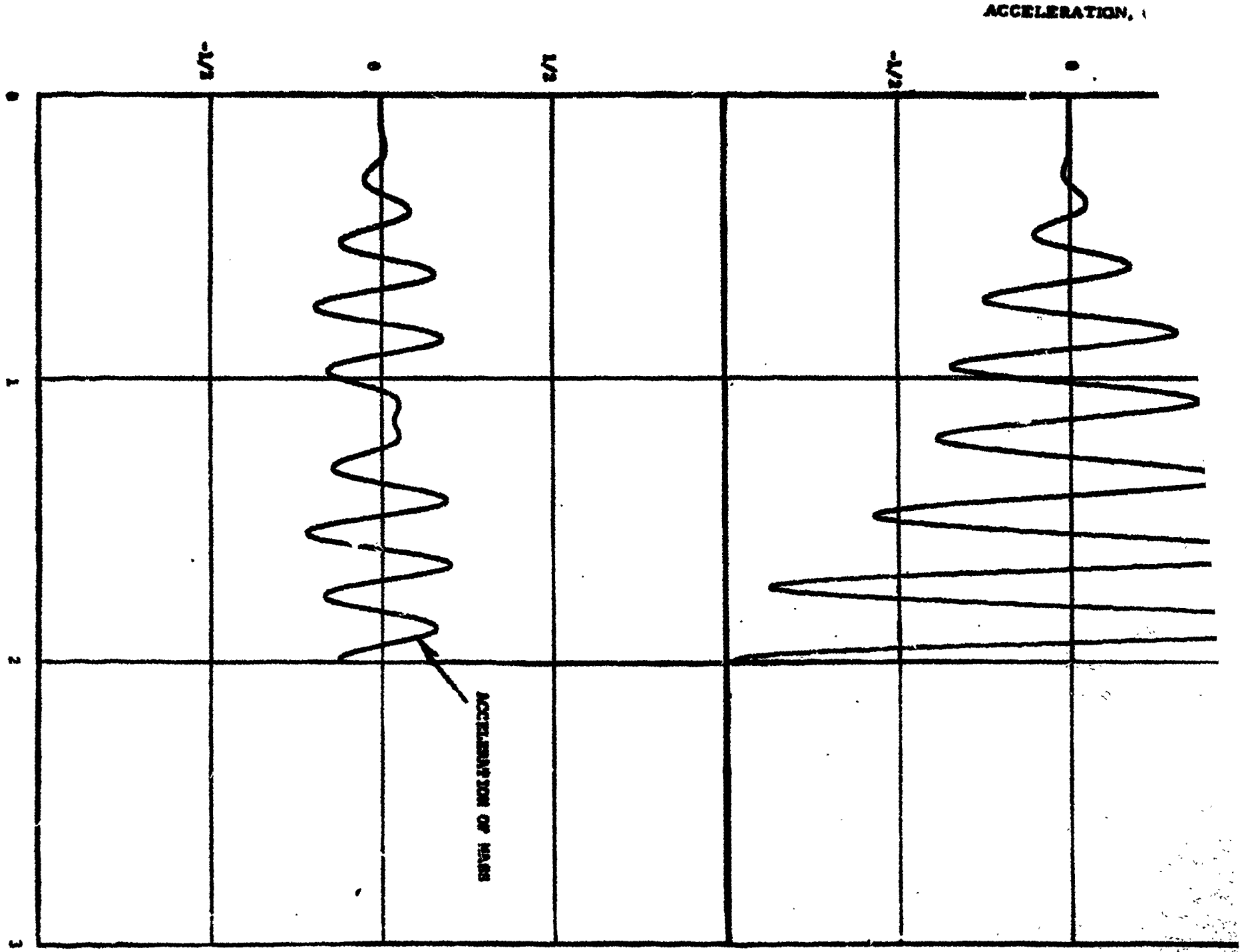

Figure 21 The lateral contribution of the acceleration, bution of the acceleration at a height of 133 fe acceleration of the containment vessel mass, calculation designated as Surface Model II is function of time. It should be noted that the lateral effects are out of phase.

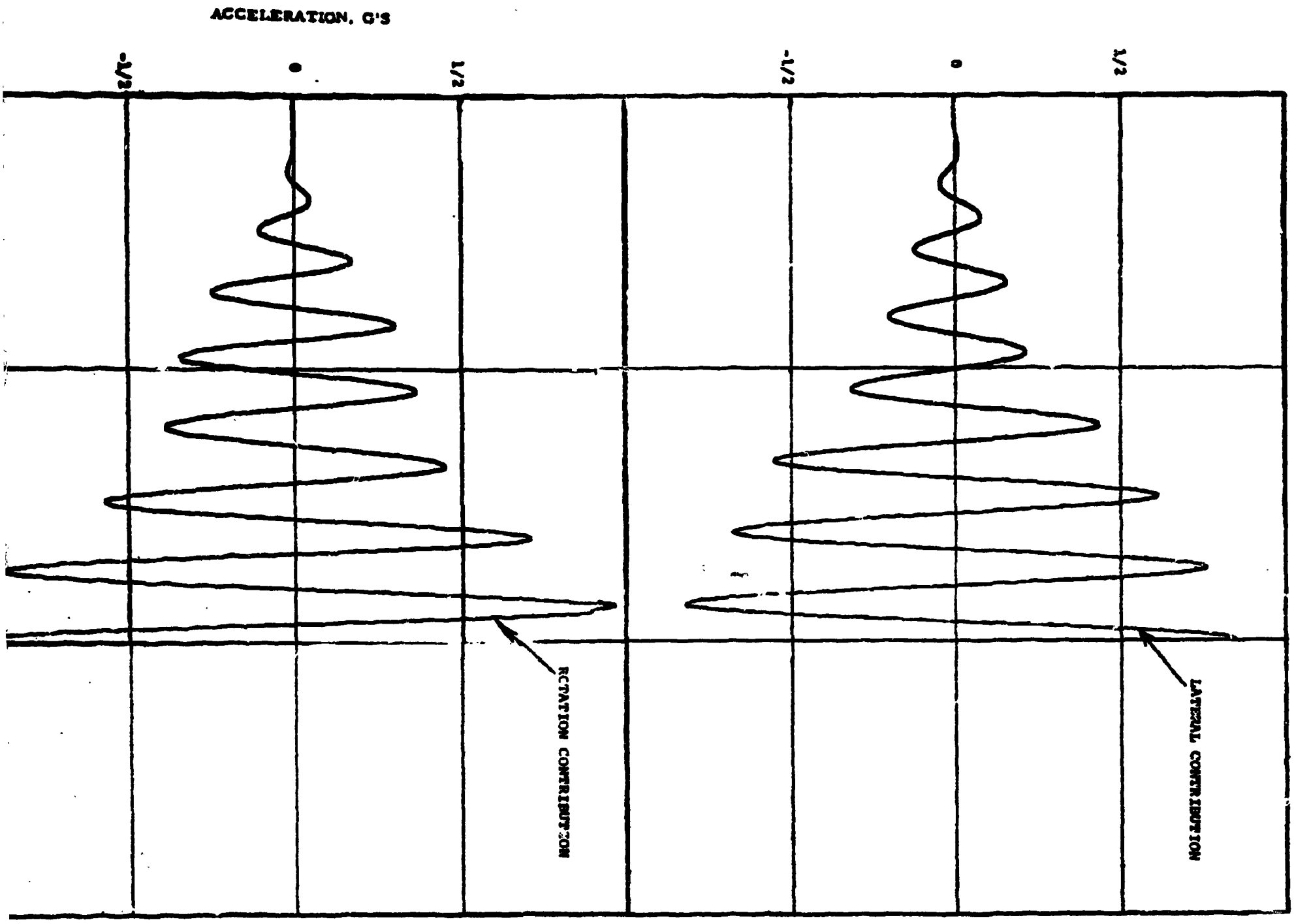

ure 21 The lateral contribution of the acceleration, the rocking contribution of the acceleration at a height of 133 feet and the acceleration of the containment vessel mass for the IITRI calculation designated as Surface Model II is shown as a function of time. It should be noted that the rocking and lateral effects are out of phase.

TABLE VIII
COMPARISON OF STRUCTURE ACCELERATIONS CAUSED BY ROTATIONAL AND LATERAL FOUNDATION MOTIONS

Frequency cps	Structure * Description	Height ft.	Accelerations, g's			
			Lateral Contribution	Rotational Contribution	Structure Acceleration	Free-field Acceleration
4.06	Surface Model I	133	0.83	0.95	0.12	2.53
4.06	Surface Model I	66.5	0.83	0.47	0.37	2.53
5.0	Surface Model I	55	0.26	0.21	0.23	1.48
5.0	Surface Model I	27.5	0.26	0.10	0.22	1.48
4.06	Surface Model II	133	0.85	0.97	0.22	2.53
4.06	Surface Model II	66.5	0.85	0.48	0.36	2.53
5.0	Surface Model II	55	0.48	0.40	0.72	1.48
5.0	Surface Model II	27.5	0.48	0.20	0.62	1.48
4.06	Embedded Model	133	0.99	0.87	0.35	2.53
4.06	Embedded Model	66.5	0.99	0.44	0.56	2.53
5.0	Embedded Model	55	0.33	0.15	0.28	1.43
5.0	Embedded Model	27.5	0.33	0.07	0.27	1.43

* Foundation motions calculated by IITRI using the SLAM Code are listed in Appendix B of Reference (8). Structure descriptions are those used in Reference (8)

The largest dynamic moment on the foundation is caused by the containment vessel mass because it is larger in magnitude than the other dynamic mass and it is more than twice as high. As a result, rocking effects are dominated by the containment structure mass and it is at the fundamental frequency of this structure that the rotational motion is out-of-phase with the lateral motion. At 4 cps, the peak structure acceleration is always much less than either the lateral acceleration or rocking contribution at a height of 133 feet.

It is concluded from this study that accelerations caused by rotation of the base are similar in magnitude to those caused by lateral motion and, therefore, must be included in all seismic analyses. Calculations which are based on a lateral spectrum response would not include these effects. Moreover, an analysis which is based upon a rotational spectrum response can not be employed because the phase relationships between lateral and rocking motions would not be considered. The effect of foundation rotation is to reduce the accelerations at the fundamental frequency of the largest dynamic mass. At other locations and frequencies, maximum accelerations can be larger than either the lateral contribution or rocking contribution alone. Furthermore, light weight equipment structures attached to the containment vessel can experience a resonant condition because of rotational motion (3).

The purpose of the analytical studies conducted under this phase of the contract was to determine the extent to which large reactor structures interact with free-field ground motions so as to alter the base motion of the structure locally from free-field values. In all cases the soil was modeled as a two-dimensional homogeneous isotropic elastic half space. Seismic free-field inputs were limited to four seconds. Longer inputs were not considered in this phase of work. Furthermore, complete coupling was assumed at the soil structure boundary. Slipping at this boundary which can be caused by soil liquefaction was not considered.

In Phase II of the contract, the influence of some of these neglected factors on soil-structure interaction is being examined. Specifically some of the factors being studied are as follows:

(1) The significance of layers in the soil

(2) The influence of time and seismic input characteristic on soil structure interaction

(3) The influence of permanent soil deformation on interaction effects

(4) The effect of slipping at the soil-structure boundary

Reports are being prepared on these items.

Results of both the analytical method of analysis and the SLAM Code results show soil-structure interaction effects are significant for low, stiff, heavy structures such as nuclear power plants. In addition, the lateral response spectrum is reduced at the foundation of this type of structure. The amount of reduction depends upon the soil stiffness, the structure weight, the structure

modal properties and the frequency characteristics of the input wave. Reductions in the lateral spectrum may be as large as a factor of 5 or may not be significant and depends upon these factors.

Structure accelerations caused by foundation rotational motion are equal in magnitude to those caused by lateral foundation motion and, therefore, must be included in seismic analyses. Moreover, accelerations caused by foundation rotation of the largest dynamic mass were found to be out-of-phase with the lateral foundation motion. As a result, peak accelerations of the mass and, therefore, seismic shock loads are reduced below the values calculated from either the lateral spectrum response or rotational spectrum response. As an example, the lateral spectrum value for Surface Model II at a frequency of 4.06 cps is 0.85 g's. The maximum acceleration of the containment vessel caused by base rotation alone is 0.97 g's. However, the peak value of acceleration of the containment vessel mass is only 0.22 g's. Thus, the lateral motion and rotational effect are out-of-phase at frequency of 4.06 cps and reduce the maximum acceleration load on the containment vessel significantly. Furthermore, this value of 0.22 g's should be compared to the free-field lateral acceleration spectrum of 2.53 g's. Thus, the total reduction from both lateral and rotational interactional effects is approximately a factor of ten.

Because of the changes in the lateral spectrum response and the acceleration caused by foundation rotation, it is concluded that seismic analyses of nuclear power plants based upon a lateral spectrum response calculated from foundation free-field motion are not accurate and should not be employed in design calculations. It is recommended that motion-time histories be determined at various elevations in a nuclear power plant considering interaction effects. Spectrum response curves

may be calculated at various elevations within a structure in order to evaluate the adequacy of light weight components located at those elevations. Major equipment structures should be included in soil-structure interaction calculations.

BIBLIOGRAPHY

1. Holmes and Narver, Inc. "Nuclear Reactors and Earthquakes." TID-7024, Aug. 1963

2. Blume, J. A., N. W. Newmark, and L. H. Corning. "Design of Multi-Story Reinforced Concrete Buildings for Earthquake Motions," Portland Cement Association, Chicago, Ill. 1961

3. Hansen, Robert J. "Seismic Design of Nuclear Power Plants," MIT Press, Cambridge, Massachusetts. 1970

4. John A. Blume and Assoc. "Summary of Current Seismic Design Practice for Nuclear Reactor Facilities," Sept. 1970

5. Scavuzzo, R. J. and J. L. Bailey, D. D. Raftopoulos. "Lateral Structure-Foundation Interaction of Nuclear Power Plants During Earthquake Loading," USAEC Contract No. AT-(40-1)-3822, Report No. 2, Research Foundation, Dept. of Mechanical Engineering of The University of Toledo, August, 1969

6. Scavuzzo, R. J. and D. D. Raftopoulos, J. L. Bailey. "Lateral Structure-Foundation Interaction of Nuclear Power Plants with Large Base Masses," USAEC Contract No. AT-(40-1)-3822, Dept. of Mechanical Engineering of The University of Toledo, Report No. 3, September, 1969

7. Scavuzzo, R. J. and J. L. Bailey, D. D. Raftopoulos. "Lateral Structure Interaction With Seismic Waves," Accepted for Publication, Journal of Applied Mechanics, 1970.

8. Chiapetta, R. "Effect of Soil-Structure Interaction on the Response of Reactor Structures to Seismic Ground Motion," IIT Research Institute, ORO-3822-4

9. Scavuzzo, R. J., "Foundation-Structure Interaction in the Analysis of Wave Motions," Bull. Seismological Soc. of America, Vol. 57, No. 4, August 1967, pp. 735-746

10. Baron, M. L. and Parnes, R., "Diffraction of a Pressure Wave by a Cylindrical Shell in an Elastic Medium," Proceedings of the Fourth U. S. National Congress of Applied Mechanics, Vol. 1, pp. 63-75, June 1962

11. Yoshihara, T. Robinson, A. R. and Merritt, J. L., "Interaction of Plane Elastic Waves with an Elastic Cylindrical Shell," Civil Engineering Studies, Structural Research Series, No. 261. University of Illinois, January 1963.

12. Scavuzzo, R. J., "Letter Progress Report No. 16" USAEC Contract No. AT(40-1)-3822, November 1969